## Gravel threshold of motion: A state function of sediment

#### transport disequilibrium? 2

3

1

#### 4 Joel P. L. Johnson

- 5 Department of Geological Sciences, The University of Texas at Austin
- Correspondence to: joelj@jsg.utexas.edu 6

7 8

15

17

19

20

21

22

23

### Abstract

9 In most sediment transport models, a threshold variable dictates the shear stress at which non-10 negligible bedload transport begins. Previous work has demonstrated that nondimensional 11 transport thresholds  $(\tau_c^*)$  vary with many factors related not only to grain size and shape, but 12 also with characteristics of the local bed surface and sediment transport rate  $(g_s)$ . J propose a

new model in which  $q_s$ -dependent  $\tau_c^*$ , notated as  $\tau_{c(q_s)}^*$ , evolves as a power-law function of 13 14

net erosion or deposition. In the model, net entrainment is assumed to progressively remove,

more mobile particles while leaving behind more stable grains, gradually increasing  $au_{c(q_i)}^*$  and

16 reducing transport rates. Net deposition tends to fill in topographic lows, progressively leading to less stable distributions of surface grains, decreasing  $au_{c(q_s)}^*$  and increasing transport

18 rates. Model parameters are calibrated based on laboratory flume experiments that explore

transport disequilibrium. The  $au_{c(q_j)}^*$  equation is then incorporated into a simple

morphodynamic model. The evolution of  $au_{c(q_s)}^*$  is a negative feedback on morphologic

change, while also allowing reaches to equilibrate to sediment supply at different slopes.

Finally,  $au_{c(q_i)}^*$  is interpreted to be an important but nonunique state variable for

morphodynamics, in a manner consistent with state variables such as temperature in

24 thermodynamics, Deleted:

Formatted: Font: Italic

Deleted: characteristics of the flow and surrounding grains.

Formatted: Font: Italic, Subscript

Deleted: Both a conceptual model and flume experiments suggest that  $\, au_{\,c}^{\,*}\,$  should evolve as a function of local entrainment and deposition.

**Deleted:** preferentially

Deleted: s

Deleted:  $\tau_c^*$ 

Deleted:  $\tau_c^*$ 

**Deleted:** A new model is proposed for the temporal evolution of  $\tau_c^*$  as a power-law function of net erosion or deposition, which shares some similarities with the Exner

Deleted:  $\tau$ 

Deleted: -evolution

Deleted:  $\tau_c^*$ 

Deleted: acts as

Deleted: s

Deleted:  $\tau_c^*$ 

Deleted: channel morphology

Deleted: the role that

Deleted: play

Deleted: describing the evolution of

Deleted: system

Deleted:

25

1

### 1 Motivation

51

76

- Despite over a century of quantitative study (Gilbert, 1914), it often remains
- 53 challenging to predict gravel transport rates to much better than an order of magnitude
- because of the complexity of grain interactions with the flow and the surrounding grains (e.g.,
- 55 Schneider et al., 2015; Nitsche et al., 2011; Rickenmann, 2001; Wilcock and Crowe, 2003;
- 56 Chen and Stone, 2008). Predictive models for complex systems often derive utility from their
- 57 simplicity, as is the case with the widely\_used Meyer-Peter and Müller (1948) transport
- 58 equation, as modified by Wong and Parker (2006):
- 59  $q_s^* = 3.97 (\tau^* \tau_c^*)^{1.5}$  for  $\tau^* \ge \tau_c^*$  (1)
- 60 where  $q_s^*$  is a nondimensional sediment transport rate per unit width,  $\tau^*$  is a nondimensional
- shear stress imparted by the fluid on the channel bed (a Shields stress), and  $au_c^*$  is the
- 62 nondimensional threshold stress at which grains begin to move (a critical Shields stress).
- Variables are nondimensionalized as follows:

64 
$$q_s^* = \frac{q_s}{D\sqrt{\left(\frac{\rho_s}{\rho} - 1\right)gD}}$$
 (2)

$$\tau^* = \frac{\tau}{(\rho_s - \rho)gD} \tag{3}$$

- where  $q_s$  is volume sediment transport rate per unit width (m<sup>2</sup>/s), D is grain diameter (m),
- 67  $\rho_s$  is sediment density (m<sup>3</sup>/kg),  $\rho$  is water density (m<sup>3</sup>/kg), g is gravitational acceleration
- 68 (m/s<sup>2</sup>), and  $\tau$  is shear stress (Pa) In principle, these nondimensionalizations should account
- 69 for differences in grain size, fluid and sediment density and gravity, allowing meaningful
- 70 comparisons of transport and stress across different conditions. For a given grain diameter
- 71 (and constant  $\rho_s$ ,  $\rho$  and g assumed for terrestrial landscapes), the simplicity of Eq. (1) is
- 72 that it predicts transport rate using just two variables,  $\tau^*$  (a function of flow strength) and  $\tau_c^*$
- 73 (a function of many variables). In practice,  $\tau_c^*$  is often back-calculated from shear stress and
- 74 bedload transport rate, essentially making it an empirical fitting parameter for a given
- 75 transport model (e.g., Wong and Parker, 2006; Buffington and Montgomery, 1997), For
  - example, using the original dataset of Meyer-Peter and Muller (1948),  $\tau^*$  and  $q_s^*$  give best-fit

Deleted: coarse bedload

Deleted:

Deleted: ed

Deleted:

Deleted:

Deleted: -

Deleted:

Deleted: a particular sediment transport model.

Deleted:

Deleted: the

 $\tau_c^*$ =0.0495 for Eq. (1) (Wong and Parker, 2006). Other bedload transport models have been developed that do not use an absolute threshold stress below which transport is zero, but rather a "reference" stress that corresponds to a very low but non-zero transport rate (e.g. Parker, 1990; Wilcock and Crowe, 2003). For most applications the practical difference between threshold and reference stresses are negligible (Buffington and Montgomery, 1997). In the present work, threshold and reference stresses are used interchangeably.

Thresholds of motion for gravel often span an order of magnitude or more (Fig. 1). Variability in  $\tau_c^*$  greatly influences bedload flux predictions in mountain rivers because transport typically occurs close to thresholds conditions, even during large floods (Phillips et al., 2013; Parker et al., 1982; Parker and Klingeman, 1982). Previous work has demonstrated that a great many factors collectively cause  $\tau_c^*$  scatter (e.g., Buffington and Montgomery, 1997; Kirchner et al., 1990). Slope can empirically explain 34% of the variability shown in Fig. 1 data, However, other variables including the strength of turbulent velocity fluctuations, and flow depth relative to bed roughness, also vary with reach slope and have been interpreted to influence  $\tau_c^*$  mechanistically (Lamb et al., 2008). In addition, thresholds can change temporally: using field data, Turowski et al. (2011) demonstrated that threshold discharges for the start and end of bedload transport could change by an order of magnitude during a given flood event.

Although thresholds of motion may dynamically evolve over time, we suggest several reasons why an assumption of constant  $\tau_c^*$  remains ingrained in some studies. First, the traditional Shields diagram indicates that  $\tau_c^*$  is rather insensitive to particle Reynolds number once flow becomes hydraulically rough around grains (Buffington, 1999). Second, because the best estimate of a given variable is usually its average, there is a tendency to attribute variability to measurement noise and uncertainty, even when that variability may be real, understandable, and important to system dynamics (Jerolmack, 2011; Buffington and Montgomery, 1997; Chen and Stone, 2008). Third, a broadly applicable model for the temporal evolution of  $\tau_c^*$  has arguably not been developed, although progress has been made (Recking, 2012; Bunte et al., 2013; Wilcock and Crowe, 2003). Next in this section, I summarize previous work on  $\tau_c^*$  controls, suggest ways that evolving  $\tau_c^*$  may influence

**Deleted:** In practice,  $\tau_c^*$  can essentially be an empirical fitting parameter for a given transport model (e.g., Wong and Parker, 2006; Buffington and Montgomery, 1997).

Deleted:

Deleted: ; see caption for data sources

Deleted: s

Deleted: that can

**Deleted:** ; for example, s

**Deleted:** (e.g., Buffington and Montgomery, 1997; Kirchner et al., 1990; Lamb et al., 2008).

126 gravel-bed river morphodynamics, and then propose specific hypotheses to be explored with a 127 new model for  $\tau_c^*$  evolution.

# 1.1 Previous work: mechanistic controls on $\tau_c^*$

In order to review previous work in an organized manner, factors affecting  $\tau_c^*$  are categorized as (a) grain controls, (b) bed state controls, (c) discharge controls, and (d) sediment flux controls, while acknowledging that many specific factors are interrelated and can be classified in more than one category. The literature on thresholds of motion is vast; I highlight select papers while acknowledging that many contributions are not explicitly reviewed.

Grain controls are physical characteristics of individual clasts that influence  $\tau_c^*$ . In addition to diameter and density, these include shape and angularity (e.g., Prancevic and Lamb, 2015; Gogus and Defne, 2005). By controlling surface grain size, armoring acts as a grain control (e.g., Dietrich et al., 1989; Parker and Toro-Escobar, 2002). However, the grain size distribution (GSD) of the surrounding bed has also been shown to strongly influence  $\tau_c^*$ : armoring can therefore also be a bed state control. In many mixed grain size transport models, hiding/exposure functions quantify the observation that grains smaller than the average bed surface tend to be relatively less mobile than expected based on diameter alone, while grains larger than average tend to be relatively more mobile than expected based on their diameter (e.g., Parker, 1990; Wilcock and Crowe, 2003). Spatial heterogeneity in surface GSDs, whether randomly distributed or sorted into patches, can also influence local  $\tau_c^*$  (Chen and Stone, 2008; Nelson et al., 2009). Mechanistically, contrasts in diameter between a grain and the surrounding bed affects pocket geometry. On rougher beds, grains tend to protrude less into the flow and therefore tend to be more stable (higher  $\tau_c^*$ ).

Sand content is a related GSD bed state control: increasing sand content of alluvial bed surfaces has been shown to decrease gravel thresholds of motion (e.g., Curran and Wilcock, 2005; Iseya and Ikeda, 1987; Jackson and Beschta, 1984). Wilcock and Crowe (2003) explicitly incorporated this sand dependence into their transport model:

$$\tau_{rm}^* = c_1 + c_2 e^{-c_3 F_s} \tag{4}$$

Formatted: Font: Not Bold

Formatted: Heading 2, Indent: First line: 0"

**Deleted:** Although interrelated,  $\tau_c^*$  influences can generally be classified as grain controls, "bed state" controls, and flow controls.

Deleted: grain controls

Deleted: (Chen and Stone, 2008; Nelson et al., 2009)

where  $\tau_{mm}^*$  is a reference stress (rather than an absolute threshold) for the geometric mean diameter of the bed surface GSD,  $F_s$  is the spatial fraction of sand on the bed surface, and constants  $c_1$ ,  $c_2$  and  $c_3$  were empirically calibrated from flume data to be 0.021, 0.015 and 20 respectively. These values result in  $\tau_{mm}^*$  varying between 0.021 and 0.036, which is in the range of typical  $\tau_c^*$  (Figure 1). Subsequent work has shown that the effects described by Eq. 4 are not unique to sand sizes only. Thresholds of motion for intermediate surface diameters (e.g.  $D_{50}$ ) can similarly be reduced by grains substantially smaller than the bed surface but larger than 2mm (Venditti et al., 2010; Sklar et al., 2009; Johnson et al., 2015). Mechanistically, the addition of sand or finer gravels smooths the bed surface by preferentially filling local topographic lows, which can affect pocket geometries (making it easier for larger grains to rotate out of a stable position), and also reduce local hydraulic roughness, increasing near-bed velocity and increasing drag on protruding grains.

Many studies have explored the bed state control of stabilizing structures formed by coarse grain clusters (e.g., Church et al., 1998; Strom and Papanicolaou, 2009). Other bed state controls include the degree of overlap, interlocking and imbrication among grains, and bed compaction or dilation, (e.g., Parker, 1990; Wilcock and Crowe, 2003; Sanguinito and Johnson, 2012; Buscombe and Conley, 2012; Mao, 2012; Kirchner et al., 1990; Strom and Papanicolaou, 2009; Marquis and Roy, 2012; Powell and Ashworth, 1995; Richards and Clifford, 1991; Ockelford and Haynes, 2013). By combining experimental data and a numerical model, Measures and Tait (2008) show that increasing grain-scale bed roughness tends to shelter downstream grains, reducing entrainment. Mechanistically, these factors attest to how, even if grain size does not change, grains can move from less stable to more stable configurations. Coarse grain clusters can also enhance bed stability by increasing surface roughness, tending to deepen potential grain pockets.

Flow characteristics influencing  $\tau_c^*$  include particle Reynolds number, flow depth relative to grain size, the intensity of turbulence, the history of prior flow both above and below transport thresholds, and the partitioning of stress into form drag and skin friction (e.g., Shvidchenko and Pender, 2000; Ockelford and Haynes, 2013; Schneider et al., 2015; Valyrakis et al., 2010; Celik et al., 2010) Most flow-dependent controls are not independent of the bed surface controls. For example, flow depths, turbulence and form drag depend on slope and bed roughness, while the stress history influences  $\tau_c^*$  by changing grain interlocking

Formatted: Font: Italic

Formatted: Font: Italic, Subscript

**Deleted:** Bed surface controls include the grain size distribution (GSD) of the surrounding bed,

Deleted: and

**Deleted:** , the protrusion of grains into the flow, the degree of coarse grain clustering, the bed roughness, and the reach slope

Deleted:

Deleted

Deleted: However, m

and surface roughness. Mao (2012) showed that thresholds of motion and bed roughness both evolved during hydrograph rising and falling limbs, leading to bedload hysteresis.

Recent work also suggests that sediment transport can affect  $\tau_c^*$ , with higher rates of upstream supply corresponding to more mobile sediment and lower  $\tau_c^*$  (Recking, 2012; Bunte et al., 2013). The idea that transport rate influences  $\tau_c^*$  is an intriguing feedback and the focus of the present analysis because, by definition,  $\tau_c^*$  influences transport rate (Eq. 1). Mechanistically, mobile grains impacting stationary grains have been shown to dislodge and entrain grains into the flow (Ancey et al., 2008). Empirically, Bunte et al. (2013) interpreted that lower  $\tau_c^*$  corresponded to looser beds caused by higher rates of sediment supply from upstream, and noted that the stability of bed particles can be qualitatively assessed in the field while doing pebble counts. Yager et al. (2012b) demonstrated that in-channel sediment availability varied inversely with the degree of boulder protrusion, indicating preferential filling of topographic lows by mobile sediment.

Recking (2012) compared bed load monitoring records from steep natural channels (>5% slope) to differences in sediment supply interpreted from aerial photographs of surrounding hillslopes. Channels with higher supply rates had higher transport rates for a given shear stress, consistent with a dependence of transport thresholds on supply. While stating that deriving a threshold model "taking into account the sediment input as a parameter would be difficult", Recking (2012) proposed quantitative bounds on reference stress for the end-member cases of very high sediment supply ( $\tau_{mss}$ ) and very low sediment supply ( $\tau_{m}$ ) in steep mountain channels:

$$\tau_{mss}^* = \left(5S + 0.06\right) \left(\frac{D_{84}}{D_{50}}\right)^{-1.5}$$
 (5)

$$\tau_m^* = (5S + 0.06) \left(\frac{D_{84}}{D_{50}}\right)^{4.4\sqrt{S} - 1.5}$$
 (6)

It should be noted that these reference stress equations describe transport of the  $D_{84}$  grain size-(rather than say  $D_{50}$ ), using a  $D_{84}$ -based bedload transport model (Recking, 2012). Importantly, the ratio  $D_{84}/D_{50}$  is included in Eq. 5 and 6 to represent surface armoring, which tends to vary with sediment supply (Dietrich et al., 1989), thus relating bed state controls to Formatted: Indent: First line: 0.49"

**Deleted:** In addition, recent work suggests that the amount of sediment supplied from upstream

Deleted: s

**Deleted:** Sensitivity of  $\tau_c^*$  to sediment flux is not obviously classifiable as either a flow or a bed state control

Deleted:

Deleted:

**Deleted:** This feedback is the focus of the present analysis.

Formatted: Indent: First line: 0"

supply-dependent bounds. Overall, this review of previous work suggests that numerous interrelated variables influence  $\tau_c^*$ , but also that many controls on  $\tau_c^*$  may share similar sensitivities to changing bed roughness and sediment supply.

## 1.2 Morphodynamics and hypotheses,

235

236

237

238

239

240

241

242

243

244

245

246

247

248

249

250

251

252

253

254

255

256

257

258

259

260

261

Feedback between channel morphology and bedload transport defines <u>mountain river</u> morphodynamics. The Exner equation of sediment mass <u>conservation</u> <u>quantifies how</u> transport changes correspond to topographic changes (Paola and Voller, 2005):

$$\frac{\partial z}{\partial t} = -\left(\frac{1}{1 - \lambda_p}\right) \frac{\partial q_s}{\partial x} \tag{7}$$

where z is bed elevation (vertical position), x is horizontal position, t is time, and  $\lambda_p$  is bed porosity. In this morphodynamic equation (presented for simplicity without an uplift or subsidence term), topographic equilibrium ( $\partial z/\partial t = 0$ ) is attained when the sediment flux into a reach equals the sediment flux out  $(\partial q_s/\partial x = 0)$ . Channel morphology has long been recognized to influence sediment transport. Of particular relevance to the present work, Stark and Stark (2001) proposed a landscape evolution model with a variable called channelization that is defined as representing "the ease with which sediment can flux through a channel reach", Conceptually, channelization characterizes how changes in reach morphology influence local transport rate. However, channelization is an abstract unitless number that does not correspond physically to any measureable aspects of morphology. A fundamental feedback is imposed in the Stark and Stark (2001) model: channelization evolves through time as a function of both sediment flux and of itself, resulting in a differential equation. The combination of local slope and channelization tend to asymptote towards values such that  $\partial q_s/\partial x = 0$ , i.e. transport equilibrium. For a given upstream sediment supply rate, a modeled reach can evolve to equilibrium at different slopes (for different corresponding values of channelization) because both slope and channelization affect transport rate. Interestingly, the above definition of channelization could also be applied to  $\tau_c^*$ . Because of its control on transport rates, changes in  $\tau_c^*$  should influence channel morphodynamics, both over human timescales (e.g., in response to natural and anthropogenic perturbations such as landslides,

**Deleted:** (Ancey et al., 2008)A constant  $\tau_c^*$  is commonly assumed for gravel transport calculations, perhaps for several reasons. First, the traditional Shields diagram indicates that  $\tau_c^*$  is rather insensitive to particle Reynolds number once flow becomes hydraulically rough around grains (Buffington, 1999). Second, a belief that  $\tau_c^*$  is fundamentally a material property of a grain rather than a bed state control also remains somewhat ingrained. Third, because the best estimate of a given variable is usually its average, there is a tendency to attribute variability to measurement noise and uncertainty, even when that variability may be real, its causes understandable, and its influence potentially important to system dynamics (Jerolmack, 2011; Buffington and Montgomery, 1997).

Formatted: Strong

Deleted: balance

Deleted: 4

Formatted: Indent: First line: 0"

Deleted:

**Deleted:** Sediment flux and bed elevation are functions of both position and time.

Deleted: n insightful

Deleted:

Deleted:

Deleted: ¶

floods, post-wildfire erosion, land use, changing climate) and longer timescales (landscape evolution).

The overall goal of the present work is to <u>understand and model</u> possible feedbacks among thresholds of motion, changes in transport rate, and the morphological evolution of channels. <u>First, I hypothesize</u> that variability in gravel  $\tau_c^*$  is physically meaningful, and that the implicit effects of multiple processes on  $\tau_c^*$  can collectively be accounted for in terms of sediment flux dependence. <u>Second, because changes in alluvial channel morphology are</u> strongly coupled with sediment flux (Eq. <u>7</u>), I hypothesize that the evolution of  $\tau_c^*$  can implicitly model effects of evolving channel morphology.

The paper is organized as follows. First, I propose a conceptual model for how  $\tau_c^*$  should evolve through time as a function of sediment flux (section 2.1), and then translate this model into equations (section 2.2). Next, I describe flume experiments on disequilibrium gravel transport (section 2.3), and use these experiments to empirically calibrate  $\tau_c^*$  model parameters (sections 3.1, 3.2). After that, effects of  $\tau_c^*$  evolution on river channel morphodynamics are explored using a simple model for river channel longitudinal profile development (section 3.3). Finally, I argue that  $\tau_c^*$  is one of many morphodynamic "state variables" that describe how river channels evolve in response to external forcing and internal feedbacks, analagous to state variables in thermodynamics (section 4.2).

## 2 Models and Methods

287

288

289

290

291

292

293

294

295

296

297

298

299

300

301

302

303

304

305

306

307

308

309

310

311

312

313

314

## 2.1 Conceptual\_framework for $\tau_c^*$ evolution

The  $\tau_c^*$  model proposed below is designed to be applicable at the reach scale, over timescales ranging from changing discharge during floods to the morphodynamic evolution of channels and surrounding landscapes. By definition, models are useful representations of reality because many complexities are omitted. Although recent work demonstrates a richness of threshold and transport behavior caused by turbulent velocity fluctuations and the statistical mechanics of particle populations over short timescales (e.g., Schmeeckle and Nelson, 2003; Diplas et al., 2008; Furbish et al., 2012), these dynamics are not explicitly considered or parameterized in my deterministic model formulation.

Deleted: elucidate

Deleted:

Deleted: A motivating hypothesis is

Deleted: both

Deleted:

**Deleted:** reflects changes in  $\tau_c^*$  as a predictable function of sediment flux. Another hypothesis is

Deleted: B

Deleted: 4

Deleted: also

Deleted:

Deleted: ¶

Deleted:

Deleted: a conceptual model

Deleted: for why

Deleted: depend on

**Deleted:** is presented

Deleted: followed by

Deleted:

**Deleted:** mixed grain size

Deleted: are used

**Deleted:** The experimental data are consistent with the Wilcock and Crowe (2003) hiding function that predicts transport rates for grain size mixtures. A simple morphodynamic model is then used to evaluate how evolving  $\tau_c^*$  influences timescales of channel profile

**Deleted:** in the discussion section

Deleted: is argued to be

Deleted: can

**Deleted:** . Comparisons are made

Deleted:

Deleted: ¶

Formatted: Font: Not Bold

Deleted:

Formatted: Font: Not Bold

349

350

351

352 353

354

355 356

357

358 359

360

361

362

363

364

365

366

367 368

369

370 371

372 373

375

separate models for every isolated control on  $\tau_c^*$  would be informative, it would also be difficult to combine myriad process-specific models and still meaningfully predict the temporal evolution of  $\tau_c^*$  for the morphodynamic evolution of channels. Rather than being a process "splitter", I approach the problem as a process "lumper": I hypothesize that many factors affecting grain mobility share common underlying dependencies on net entrainment and net deposition.

Section 1.1 shows that a great many variables and processes influence  $\tau_c^*$ . While

Consistent with the form of most bedload transport equations (e.g. Eq. 1),  $\tau_c^*$  is defined as a particular Shields stress at which only the most mobile grains of that size become entrained. However, for a population of grains of a given size on the bed surface, there should actually be a distribution of  $\tau_c^*$ —notated here as a set of values  $\{\tau_c^*\}$ --because each individual grain has a particular pocket geometry and near-bed flow velocity at its unique location, and hence a somewhat different individual threshold. Gravel flux increases with discharge primarily because thresholds are gradually exceeded for increasing proportions of surface grains of a given size. For a given transport equation (e.g. Eq. 1), a particular  $\tau_c^*$  value from the lower tail of distribution  $\{\tau_c^*\}$  should best predict sediment flux. Conceptually, an underlying assumption is that net entrainment or net deposition changes the underlying  $\{\tau_c^*\}$ distribution, and therefore changes the value of  $\tau_c^*$  that best predicts transport rates.

In the case of a channel reach undergoing net erosion ( $q_{sout} > q_{sin_{\pi}}$ ), the most mobile <u>individual</u> grains—i.e. the <u>lowest</u>  $\tau_c^*$  <u>values in the</u>  $\{\tau_c^*\}$  <u>distribution--</u>would preferentially be entrained first, while the grains remaining on the bed would tend to have higher thresholds. Therefore, I hypothesize that progressive erosion tends to entrain grains from increasingly more stable positions on the bed, gradually increasing  $\tau_c^*$ . Conversely, during net deposition  $(q_{sout} \le q_{sin})$ , <u>I assume that</u> grains tend to preferentially deposit in more stable bed positions such as local topographic lows. Continued deposition would lead to grains being deposited in progressively less stable positions, gradually decreasing  $\tau_c^*$ . These hypothesized  $\tau_c^*$  changes represent averages for the population of grains; individual grains would exhibit great

Formatted: Not Highlight

**Deleted:** For bed surface grains of a given size class,  $au_c^*$ actually represents the stress at which only the most mobile of those grains become entrained. Individual grains will each have a different threshold based on the pocket geometry and near-bed flow velocity at its particular location, resulting in  $\tau_c^*$  probability distributions when considering all similarly sized grains (Kirchner et al., 1990; Buffington et al., 1992). Gravel flux increases with discharge primarily because thresholds are gradually exceeded for increasing proportions of surface grains of a given size. When the sediment flux entering a reach—  $q_{\rm sin}$  —is balanced by the flux exiting  $q_{\mathit{sout}}$  —it is assumed that the  $au_{\mathit{c}}^*$  probability distribution does not change over time, and that  $\tau_c^*$  remains constant.

**Deleted:**, so  $\partial q_s / \partial x > 0$ 

Deleted: P

Deleted: will

Deleted:

Deleted: will

Deleted:

variability. For example, during net deposition individual grains would also both deposit and be entrained from more and less stable positions, but grains would have a greater probability of remaining deposited in the more stable positions.

Mechanistically,  $\tau_c^*$  evolution would also be driven by changes in bed topography and roughness, grain clustering and stabilizing structures, compaction of the bed and interlocking of grains, etc. None of these physical variables are explicitly included in the model equations; instead their combined effects are assumed to vary with net erosion or deposition. Importantly, the amount by which  $\tau_c^*$  changes should also depend on the current state of the bed surface. For example, starting from a relatively rough and interlocked bed surface, net deposition would initially cause relatively substantial decreases in bed roughness as local lows preferentially filled with loose grains, and relatively large corresponding decreases in  $\tau_c^*$ . However, for a given surface GSD there must be physical limits for bed roughness and grain packing. If bed surface grains are already relatively loose, and mobile, additional deposition would cause less of a decrease in  $\tau_c^*$ , or no decrease at all if the bed is already as unstable for a given surface GSD as it can be. Thus, the change in  $\tau_c^*$  should also be a function of  $\tau_c^*$ . The combination of processes that cause changes in  $\tau_c^*$  also place physical limits on how high, and low,  $\tau_c^*$  can evolve.

These  $\tau_c^*$  dependencies describe negative transport feedbacks: net erosion progressively reduces rates of erosion by making grains harder to entrain, while net deposition progressively makes grains more mobile. Through these and other morphological feedbacks, it has long been recognized that channel reaches evolve towards steady-state configurations in which the sediment flux into a reach balances the flux exiting, leading to zero net erosion or deposition (Mackin, 1948). At this statistical steady state,  $\tau_c^*$  should also be at equilibrium, and in fact is a key part of reaching channel reach equilibrium. If  $\tau_c^*$  were still systematically evolving (e.g. from continued bed state changes), then transport rate through the reach would also change, perturbing the channel away from its statistical equilibrium.

**Deleted:** These changes describe negative transport feedbacks: net erosion progressively reduces rates of erosion by making grains harder to entrain, while net deposition progressively makes grains more mobile and less likely to be deposited. ¶

### Deleted:

Deleted:

Deleted: ly packed

Deleted: highly

Deleted: little additional

Deleted:

**Deleted:** On the other hand, initial deposition onto a stable bed would likely cause bigger reductions in  $\tau_c^*$  than subsequent deposition. Thus, the change in  $\tau_c^*$  should also be a function of  $\tau_c^*$ .

# 2.2 $\tau_{c(q_s)}^*$ model equations

 While the above discussion makes the case that  $\tau_c^*$  inevitably evolves through time due to a variety of interrelated factors, the new model proposed here is specifically in terms of sediment flux. I use the notation  $\tau_{c(q_s)}^*$  to distinguish this specific model from more general representations of thresholds of motion in other models and analyses. Because longitudinal coordinate x increases downstream, net erosion in a reach is indicated by  $\partial q_s/\partial x > 0$  and net deposition by  $\partial q_s/\partial x < 0$ . The following relations are proposed:

15 
$$\frac{\partial \tau_{c(q_s)}^*}{\partial t} = \begin{cases} kB \left( \left| \frac{\partial q_s}{\partial x} \right| \right)^{\kappa_{out}} & \text{if } \partial q_s / \partial x > 0 \\ -k \left( 1 - B \right) \left( \left| \frac{\partial q_s}{\partial x} \right| \right)^{\kappa_{dep}} & \text{if } \partial q_s / \partial x < 0 \end{cases}$$

46 
$$B = \frac{\tau_{c \max}^* - \tau_{c(q_i)}^*}{\tau_{c \max}^* - \tau_{c \min}^*}$$
 (9)

where  $\kappa_{ent}$  and  $\kappa_{dep}$  are dimensionless exponents corresponding to entrainment and deposition, respectively, and k is a scaling factor. These three parameters will be empirically fit to experiments.  $\tau_{c\min}^*$  and  $\tau_{c\max}^*$  represent bounds on how low or high  $\tau_{c(q_s)}^*$  can plausibly evolve (assumed to be 0.02 and 0.35 respectively). Eq. (8) predicts that  $\tau_{c(q_s)}^*$  incrementally decreases with net deposition, and incrementally increases during net erosion. "Feedback factor" B has a value between 0 and 1 and makes Eq. (8) a differential equation. It scales the incremental change in  $\tau_{c(q_s)}^*$  so that deposition on an already "loose" bed ( $\tau_{c(q_s)}^*$  close to  $\tau_{c\min}^*$ ) minimally decreases  $\tau_{c(q_s)}^*$ , but erosion causes a larger  $\tau_{c(q_s)}^*$  increase. Conversely, if  $\tau_{c(q_s)}^*$  is already high (close to  $\tau_{c\max}^*$ ), then erosion causes a much smaller  $\tau_{c(q_s)}^*$  change than deposition. Finally, I note that representing  $\partial \tau_{c(q_s)}^*/\partial t$  as a function of  $\partial q_s/\partial x$  (Eq. 8) is broadly analogous in form to Exner (Eq. 7).

#### Deleted: ¶

<#>Two additional points need to be made. First, natural sediment is a mixture of sizes. It is common to assume that a single representative grain size, such as the median ( $D_{50}$ ), adequately describes transport of the whole mixture. Second, "thresholds" can represent different things in different models. In Eq. (1),  $\tau^* = \tau_c^*$  represents a modeled transport rate of zero. In other models designed to predict measurable transport rates at very low shear stresses, a non-threshold "reference" stress is instead defined as the Shields stress at which  $q_s^*$  has a very low but specific nonzero value (Parker, 1990; Wilcock and Crowe, 2003). For many applications the practical difference between threshold and reference stresses are negligible (Buffington and Montgomery, 1997), and in the present work they are largely used interchangeably. ¶

largely used interchangeably.  $\P$ Formatted: Font: Not Bold

Formatted

Deleted:  $\tau_c^*$ ...-evolution

**Deleted:** deposition in a reach is indicated by  $\partial q_s/\partial x < 0$  ...nd local ...et deposition by

Poleted: ... ... ...

Formatted: Highlight

Deleted: 6

Formatted: Highlight

**Formatted** 

**Deleted:** ...These three parameters will be empirically fi

A limitation of Eq. (8) is that, for dimensional consistency, the units of k vary with  $\kappa_{ent}$  and  $\kappa_{dep}$ . An improved equation replaces spatial changes in flux with spatial changes in

the thickness of deposited or eroded sediment:

$$\frac{\partial \tau_{c(q_s)}^*}{\partial t} = \begin{cases}
kA_r B \left( \left| \frac{\partial \theta_s}{\partial x} \right| \right)^{\kappa_{cmt}} & \text{if} \quad \partial q_s / \partial x > 0 \\
-kA_r \left( 1 - B \right) \left( \left| \frac{\partial \theta_s}{\partial x} \right| \right)^{\kappa_{dep}} & \text{if} \quad \partial q_s / \partial x < 0
\end{cases}$$
(10)

640  $\theta_s$  is the thickness of sediment deposited or eroded at a given location.  $\partial \theta_s/\partial x$  is a

dimensionless ratio representing spatial changes in erosion and deposition. In this case, k has

dimensions 1/t and scales how quickly  $\tau_{c(q_s)}^*$  evolves.  $\theta_s$  can be calculated by integrating Eq.

543 (7) over time interval  $t_1$  to  $t_2$ :

538

545

546

548

549

550

551

$$\theta_s(t_2, x) = z(t_2, x) - z(t_1, x) = \frac{1}{1 - \lambda_n} \int_{1}^{t_2} \frac{\partial q_s(t, x)}{\partial x} dt$$
 (11)

(recall that  $\int_a^b (\partial f(s,t)/\partial t) dt = f(s,b) - f(s,a)$  for a generic function f). Using discrete flume

data,  $\theta_s$  is calculated over a measurement interval  $\Delta t$  as  $(1-\lambda_p)^{-1}(\overline{q_{sout}}-\overline{q_{sin}})\Delta t/\Delta x$ , where

547  $\Delta x$  is the length of the flume and the sediment flux terms are averaged over  $\Delta t$ .

A<sub>r</sub> is a dimensionless armoring parameter, calculated in several ways in order to

explore whether predictions can be improved by explicitly including bed surface grain size or

<u>bed roughness characteristics. Setting</u>  $A_r = D_{50}/D_{84}$  (the reciprical of the Recking (2012)

armoring constraint in Eq. 5 and 6) means that incremental changes to  $\tau_{c(q_s)}^*$  are larger where

552  $\underline{D}_{50}$  is relatively closer to  $\underline{D}_{84}$ . Setting  $A_r = 2D_{50}/(D_{84} - D_{16})$  suggests that  $\tau^*_{c(q_s)}$  changes

should be larger when intermediate diameters are large relative to a measure of the

normalized width of the bed surface GSD. I also try  $A_r = D_{50}/\sigma$ , where  $\sigma$  is bed surface

roughness.  $A_r = D_{50}/\sigma$  suggests that, relative to topographic lows and highs, large grains

cause bigger  $\tau_{c(q_s)}^*$  changes than small grains. Finally,  $A_r$  is simply set to 1 in some

557 <u>calculations below.</u>

Deleted: 5

Deleted: ly

Deleted:

Deleted: 7

**Deleted:**  $A_r$  is an optional dimensionless armoring parameter, described further below.  $\theta_{\rm s}$ 

**Deleted:** ; it has dimensions of length

Deleted:  $\tau_c^*$ 

Deleted: 4

Deleted: 8

**Deleted:** While  $A_r$  is set to 1 for many calculations below, the parameter is

**Deleted:** Recking et al. (2012)

Formatted: Font: Italic

Formatted: Font: Italic, Subscript

Formatted: Font: Italic

Formatted: Font: Italic, Subscript

**Deleted:** included in order to explore whether other metrics of relative surface grain size variability or bed roughness improve predictions. For example, the rate at which  $\tau_c^*$  changes might depend on grain size relative to bed surface roughness ( $\sigma$ ), i.e.  $A_r = D_{50}/\sigma$ . Setting  $A_r = D_{50}/\sigma$  suggests that, relative to topographic lows and highs, large range cause bigger  $\tau_c^*$  changes than small

## 2.3 Experimental design

579

580

581

582

583

584

585

586

587

588

589

590

591

592

593

594

595

596

597

598

599

600

601

602

603

604

605

606

607

608

609

The flume experiments used to calibrate k,  $\kappa_{ent}$  and  $\kappa_{dep}$  were designed to explore feedback during disequilibrium transport in gravel-bed rivers. Fig. 2 shows how transport rates, surface D<sub>50</sub> and bed slope evolved in response to fine gravel pulses. Johnson et al. (2015) provide details of the experimental conditions and how they scale to natural conditions most consistent with step-pool development, and so the summary here is brief. Four experiments were conducted in a small flume 4 m long and 10 cm wide Experiments 1 and 4 were done at 8% initial slope, and 2 and 3 at 12% initial slope; slopes subsequently evolved fairly little during morphological adjustment (Fig. 2c). Water discharge was held constant throughout to better isolate the influence of sediment supply changes on transport. Sediment transported out of the flume was caught in a downstream basket, sieved and weighed. Overall sediment diameters ranged from 0.45 to 40 mm; these sizes were sorted and painted different colors based on five size classes with  $\underline{D}_{50} = 2.4, 4.5, 8.0, 15.4, \text{ and } 27.2 \text{ mm}$   $\underline{(D}_{16} = 2.0, 3.4)$ <u>6.7, 12.4, and 24.0 mm;  $D_{84} = 2.8, 5.7, 10.3, 19.7, and 31.3 mm, respectively</u>). Surface GSDs</u>$ were measured using image analysis of colored bed surface grains during the experiments. Bed topography was measured using a triangulating laser, and bed roughness ( $\sigma$ ) was calculated from longitudinal topographic swaths as the standard deviation of detrended bed elevations. Water surface elevations were measured using an ultrasonic distance sensor, and water depths were calculated by subtracting bed elevations. Total shear stress  $(\tau)$  was calculated assuming steady uniform flow when spatially averaged over the flume:

 $\tau = \rho g h S \tag{12}$ 

where h is water depth corrected for sidewall effects following the method of Wong and Parker (2006), and S is water surface slope.

The experiments started with mixed-size sediment screeded flat. Initially, all surface sizes were observed to be mobile (and therefore above thresholds of motion). At the beginning no sediment was fed into the upstream end ( $q_{sfeed} = 0$ ), and the bed responded by coarsening, roughening and gradually stabilizing as transport rates dropped by  $\approx 3$  orders of magnitude (Fig. 2a). After this initial stabilization, a step-function pulse of the finest gravel size ( $D_{50}=2.4$  mm) was fed into the flume at  $q_{sfeed} \equiv 1000$  g/min, representing an idealization of a landslide, debris flow, post-wildfire erosion, or anthropogenic gravel augmentation that would suddenly supply sediment finer than the existing bed surface. The feed rate was chosen

Formatted: Font: Not Bold

**Deleted:** The flume experiments used to calibrate k,  $K_{em}$  and  $K_{dep}$  explore how fine gravel pulses influence the morphodynamics of step-pool like channels.

Formatted: Font: Italic

Formatted: Font: Italic, Subscript

Deleted:

Deleted:

**Deleted:** over different time intervals

Deleted: Sediment was

**Deleted:** median diameters

Formatted: Font: Italic

Formatted: Font: Italic, Subscript

Formatted: Font: Italic

Formatted: Font: Italic, Subscript

Deleted:

Deleted: 9

Deleted:

Deleted: grain

**Deleted:** some net erosion. The bed

Deleted: stabilized

Deleted: and

**Deleted:** to be very low

**Deleted:** bed

**Deleted:**, or similar process

**Deleted:** a prolonged pulse of

to be similar to the high initial transport rates (Fig. 2a), while not so high as to inhibit morphodynamic feedback by fully burying the existing bed surface. Initially some deposition occurred on the bed, but the channel adjusted rapidly, by both entraining coarser bed surface grains and transporting most of the finer supplied gravel, so that the outlet transport rate  $(q_{sout})$  approximately matched  $q_{sin}$ . After the sediment supply pulse  $q_{sin}$  was again dropped to zero, and the bed gradually restabilized. Johnson et al. (2015) explained in detail how bed roughness evolved, and how the addition of finer gravels ultimately caused surface coarsening (Fig. 2b). Unbalanced transport rates into and out of the flume demonstrate disequilibrium conditions (Fig. 2a), although transport evolved towards equilibrium.

## 2.4 The Wilcock and Crowe (2003) transport model

629

630

631

632

633

634

635

636

637

638

639

640

641

642

643 644

645

646

647

648

649

650

651

653

654

655

To quantify thresholds of motion from these experimental data (Fig. 2) requires a transport model. The Wilcock and Crowe (2003) "Surface-based Transport Model for Mixed-Size Sediment", abbreviated as W&CM, is used for two main reasons. First, the model can, at least in principle, account for the effects of changing surface GSD on  $\tau_c^*$ . Second, the model should also be able to account for possible effects of sand and fine gravel abundance on thresholds of motion (Eq. 4). By using the W&CM to isolate and remove GSD effects, experimentally-constrained thresholds of motion can then be used to evaluate the proposed  $\tau_{c(q_i)}^*$  functions (Eq. 8-11). A secondary goal is to evaluate how well the W&CM predicts disequilibrium transport at steeper slopes and lower water depths than Wilcock and Crowe (2003) used in their own steady-state experiments.

A <u>key</u> variable in the W&CM is  $\tau_{rs50}^*$ , the <u>nondimensional</u> reference stress for the median surface grain size  $(D_{s50})$ .  $\tau_{rs50}^*$  corresponds to a very low transport rate of  $W_i^* = 0.002$ .  $W_i^*$  is a nondimensional bedload transport rate for grain size class i,

$$652 W_i^* = \left(\frac{\rho_s}{\rho} - 1\right) \frac{gq_{bi}}{F_i u_\tau^3} (13)$$

where  $q_{bi}$  is the volumetric transport rate per unit channel width of grains of size i,  $F_i$  is the fraction of size i on the bed surface, and  $u_{\tau}$  is shear velocity  $(u_{\tau} = \sqrt{\tau/\rho})_{\tau}$ . Wilcock and Crowe (2003) presented an empirical relationship between transport and shear stress:

Deleted: t

**Deleted:** , asymptotically approaching though not quite attaining equilibrium transport (  $q_{sout} \approx 0$  ) during the remainder of each experiment.

Formatted: Heading 2, Indent: First line: 0"

Deleted: ¶

Formatted: Font: Not Bold

**Deleted:** As described above,  $\tau_c^*$  is often calculated by fitting a sediment transport model to data.

**Deleted:** Experimental shear stresses and GSDs provide all of the variables needed to evaluate the "Surface-based Transport Model for Mixed-Size Sediment" of

Deleted: A

Deleted: can

**Deleted:** in the present experiments, which used

Deleted: reach

Deleted: and

Deleted: relative to GSDs compared to experiments of

**Deleted:** In addition, disequilibrium transport was intentionally quantified during supply perturbations that caused net deposition or erosion. In contrast, the experiments Wilcock and Crowe (2003) used to calibrate their model intentionally reflected steady-state transport.

Deleted: central

Deleted:  $au_{rs50}$ 

Formatted: Font: Not Italic

**Deleted:** The nondimensional equivalent is  $\tau_{rs50}^*$  (Eq. 3). Rather than being an actual threshold (i.e.,  $\tau_c^*$ ),

Deleted: 10

$$683 W_{i}^{*} = \begin{cases} 0.002 \left(\frac{\tau}{\tau_{ii}}\right)^{7.5} & for \quad \tau/\tau_{ii} < 1.35 \\ 14 \left(1 - \frac{0.894}{\left(\frac{\tau}{\tau_{ii}}\right)^{0.5}}\right)^{4.5} & for \quad \tau/\tau_{ii} \ge 1.35 \end{cases}$$

where  $\tau_{i}$  is a dimensional reference stress for size class i, with dimensionless equivalent  $\tau_{i}^{*}$ 

685 (Eq. 3). A "hiding function" determines how nondimensional reference stresses vary with

686 grain size:

689

692

695

697

699

700

$$\frac{\tau_{ri}^*}{\tau_{rs,50}^*} = \left(\frac{D_i}{D_{s,50}}\right)^{b-1} \tag{15}$$

The hiding function exponent b is calculated as

$$b = \frac{0.67}{1 + e^{(1.5 - D_l/D_{s50})}} \tag{16}$$

Note that Eq. (16) is slightly modified from the exact Wilcock and Crowe (2003) version by

replacing  $D_{sm}$  (the geometric mean surface diameter) with  $D_{s50}$ , to more simply use just one

measure of the central tendency of the surface GSD.

## 693 3 Results

In this section, the W&CM is used to calculate best-fit thresholds of motion, Next, the

 $au_{c(q_s)}^*$  model is shown to predict the experimentally-constrained  $au_{rs50}^*$  trends after calibrating

several parameters. Finally, the influence of  $\tau_{c(q_s)}^*$  on morphodynamics is explored using a

simple model for gravel-bed river profile evolution.

## 698 3.1 Best-fit $\tau_{rs50}^*$ and hiding functions

The experimental data are used to determine  $W_i^*$  (Eq. 13) and  $\tau_{ii}^*$  for each of the five-

grain size classes (Eq. 14). Best-fit  $\tau_{rs50}^*$  is then calculated in two ways. In the first approach,

701 b is calculated using Eq. (16), and  $\tau_{rs50}^*$  and 95% confidence intervals are estimated using

702 nonlinear multiple regression in Matlab (Fig. 3, "W&CM fit"). Importantly, the temporal

Deleted: 11

Deleted: 12

Deleted: H

Deleted: 13

**Deleted:** the W&CM b relation was

**Deleted:** The additional dependence of  $\tau_{rs50}^*$  on surface sand fractions in this model will be addressed below.¶

**Deleted:** Johnson et al. (2015){Johnson, 2015 #4610}

Formatted: Normal, Indent: First line: 0.5"

Deleted: ¶

Experimental data and b

Formatted: Font: Not Bold

Deleted:

Formatted: Font: Not Bold

Deleted: Transport rates, surface grain size, and reach slopes evolved during the experiments as the flume beds initially stabilized, then responded to the pulse of sediment supply, and finally restabilized (Fig. 2). Johnson et al. (2015) explained in detail how the addition of gravels finer than the stabilized bed surface ultimately caused further surface coarsening. Relevant to the present analysis, transport rates in and out of the flume are not always balanced (Fig. 2a), although transport evolves towards this equilibrium condition.

Formatted: Indent: First line: 0.49"

Deleted: 0

Deleted: then

Deleted: 1

Deleted: simply

Deleted: 13

Deleted: N

Deleted: (

Deleted: )

**Deleted:** is then used for best-fit parameter estimation of  $\tau_{rs50}^*$  and 95% confidence intervals for each experimental time step

**Deleted:** A key point to emphasize is that e

evolution of best-fit  $\tau_{rs50}^*$  is not explained by grain size changes, because the W&CM already accounts for the effects of surface GSD (Fig. 3).

While b varies with relative grain size in the W&CM (Eq. 16), other proposed hiding functions have found (or assumed) that a single b value applies to different grain sizes, at least for a given set of flow and surface conditions (Parker, 1990; Buscombe and Conley, 2012). My second approach for estimating  $\tau_{rs50}^*$  explores whether the results are sensitive to the particular form of Eq. (16), Rather than Eq. (16), nonlinear multiple regression was used to estimate both b and  $\tau_{rs50}^*$  in Eq. (15), with separate regressions for each time step (Fig. 3). The temporal evolution of experimental  $\tau_{rs50}^*$  is generally comparable for the two different approaches (Fig. 3).

Interestingly, Fig. 4 shows that the hiding function exponents determined using the nonlinear multiple regressions for b and  $\tau_{rs50}^*$  are consistent with Eq. (16) of Wilcock and Crowe (2003). In spite of substantial scatter there is a slope break which corresponds to a change in b for surface grains smaller and larger than the median, suggesting that the W&CM reasonably can describe hiding and exposure relations among grains in steeper channels and for shallower flow depths than used in the Wilcock and Crowe (2003) experiments.

## 3.2 Calibration of $\tau_{c(q_s)}^*$ model parameters

736

737

738

739

740

741

742

743

744

745

746

747

748

749

750

751

752

753

754

755

756

757

758

759

760

761

762

Fig. 5 compares experimentally-constrained thresholds of motion to several predictions of these trends. First, I test whether surface sand fraction (Eq. 4) can explain the evolution of  $\tau_{rs50}^*$  (Curran and Wilcock, 2005; Wilcock and Crowe, 2003). As described in section 1.1, the effect of finer grains on thresholds of motion of coarser grains is not limited to sand sizes alone (Venditti et al., 2010; Sklar et al., 2009; Johnson et al., 2015). In the Johnson et al. (2015) experiments, the finest grain size class has  $D_{50}$ =2.4 mm,  $D_{10}$ =2.0 mm,  $D_{84}$ =2.8 mm. Setting  $F_8$  equal to the surface fraction of this size class, a nonlinear multiple regression of Eq. (4) to all four experiments together yielded a poor although statistically significant fit to the data ( $R^2$ =0.13; P=3x10<sup>-5</sup>;  $c_1$ =0.097±0.04,  $c_2$ =0.103±0.11, and  $c_3$ =5.6±11), confirming that surface grain size changes alone cannot explain observed  $\tau_{rs50}^*$  patterns (Fig. 5, "Sand

Deleted: xperimental ...rain size changes do not explain ...

**Deleted:** Also note that a form drag correction was not done; transport was calculated in terms of total stress (Eq. 9; section 5.5).

Formatted: Highlight

**Deleted:** hiding function exponent ... varies with relative

**Deleted:** The v second approach for estimating  $au^*$  ...

### **Formatted**

**Deleted:** Although the 95% confidence intervals tend to be larger because both b and  $\tau_{rs50}^*$  were estimated rather than just  $\tau_{rs50}^*$ , t...he temporal evolution of experimental  $\tau_{rs5}^*$ .

**Deleted:** these experiments are ...onsistent with Eq. (16) ... **Deleted:** (Eq. 13)... Fig. 4 shows data points determined

Formatted: Font: Not Bold

**Deleted:**  $\tau_c^*$  ...-evolution

Formatted: Indent: First line: 0.4"

**Deleted:** the experiment and W&CM-based calculation of  $\tau_{rs50}^*$  ... to several predictions of these trends.

**Deleted:** a sand fraction dependence is explored.

## Formatted

**Deleted:** A unique aspect of the W&CM not described above is that changes in surface sand fraction could cause temporal evolution of  $\tau_{rs50}^*$ . In particular, Wilcock and

Crowe (2003) proposed that  $\tau_{rs50}^*$  varied systematically from 0.036 with no surface sand to 0.021 with abundant surface sand:¶

$$\tau_{rs50}^* = c_1 + c_2 e^{-c_3 F_s} \tag{14}$$

where  $F_s$  is the fraction of sand on the bed surface, and constants  $c_1$ ,  $c_2$  and  $c_3$  were empirically found by them to be 0.021, 0.015 and 20 respectively (for simplicity, the geometric mean reference stress was again replaced in their original equation with  $\mathcal{T}_{rs50}^*$ ). Subsequent work has shown that thresholds of motion can similarly be reduced by grains substantially smaller than the bed surface but larger than sand (Venditti et al., 2010; Sklar et al., 2009; Johnson et al., 2015), suggesting that the "sand fraction" effect could also be modeled for grains larger than 2 mm. ¶ In the present experiments, the surface fraction of actual sand (<2 mm) was very small. However, because grains larger than sand but smaller than the average bed surface may also enhance mobility, we evaluate whether Eq. (14) can explain the experimentally-constrained variations in

 $\tau_{rs50}^{*}$ . Using the surface fraction of grains < 2.8 mm (representing the smallest grain size class in the experiments)

867 fraction"). Note that I have assumed for simplicity that  $\tau_{rs50}^* = \overline{\tau}_{rm}^*$ , i.e. substituting the surface 868 D<sub>50</sub> for the geometric mean surface diameter in Eq. (4). Formatted: English (United Kingdom) 869 <u>Various</u>  $\tau_{c(q_s)}^*$  models provide better fits to experimentally-constrained  $\tau_{rs50}^*$  Fig. 5: **Deleted:** My proposed arious  $\tau^*$ . 870 Eq. 10), Models with  $A_r=1$  are shown using a single set of model parameters for all four 871 experiments ("collective best fit", k=0.17,  $\kappa_{dep}=0.20$ ,  $\kappa_{ent}=0.40$ ), and also the best fit for each experiment separately. The best-fit overall model has R<sup>2</sup>=0.69, suggesting statistically that 872 873 effects of supply and transport disequilibrium can explain over 2/3 of the variability in  $\tau_{rs50}^*$ (Table 1). Note that  $\tau_{c(q_s)}^*$  and  $\tau_{rs50}^*$  are assumed to be interchangeable. Because Eq. (8) and 874 875 (10) are differential equations, best-fit parameters could not be calculated using nonlinear 876 multiple regressions. Instead, I use a brute-force approach of incrementally stepping through a 877 wide range of k,  $\kappa_{dep}$  and  $\kappa_{ent}$ , and finding the combination of parameters that give the 878 smallest root-mean-square deviation (RMSD). The se calculations started at  $\tau_{rs50}^* = 0.036$  at 879 t=0, which is consistent with the experiments, and also is the  $\tau_{rs50}^*$  proposed by Wilcock and 880 Crowe (2003) in the absence of sand dependence. Deleted: 881 Interestingly, model fits using  $A_r = D_{50}/\sigma$  are not substantially different from  $A_r=1$ , and  $R^2$ =0.69 is the same (Fig. 5). Table 1 includes additional regressions for  $\underline{for}_{84} = D_{50}/D_{84}$ 882 **Deleted:** ...Table 1 includes three ...dditional regression 883 and  $A_r = 2D_{50}/(D_{84} - D_{16})$ . These fits overlap almost perfectly with those shown on Fig. 5. 884 As explained in section 1.1, Ar should account for surface GSD and bed topography **Formatted** 885 influences on thresholds. The fact that regressions are not improved by including these 886 variables may suggest that transport disequilibrium is a more important control on threshold 887 evolution over a broad range of surface GSD and bed roughness. Parameters estimated for Deleted: fits overlap almost completely with those already shown.  $A_r = D_{s50}/D_{s84}$  was tried, because the inverse 888 dimensional  $\partial q_s/\partial x$  (Eq. 8) indicate that the dimensionally balanced model performs equally ratio Ds84/Ds50 represents the degree of armoring in the analysis of  $\tau_c^*$  supply dependence by Recking (2012).

<u>well (Table 1)</u>. Because these variants do not substantially improve  $\tau_{c(q_i)}^*$  model fits, we use

the simplest dimensionally consistent model (Eq.  $\underline{10}$  with  $A_r=1$ ) in the analysis below.

889

890

 $A_r = 2D_{s50}/(D_{s84} - D_{s16})$ 

**Deleted:** was also tried as a measure of the normalized GSD width. Finally, p...arameters  $\underline{\text{were}}\ ...\text{stimated}$  for

## 3.3 Influence of $au_{c(q_s)}^*$ on morphodynamics

952

953

954

955

956

957

958

959

960

961

962

963

964

965

Next, an idealized morphodynamic model demonstrates how the proposed  $\tau_{c(q_i)}^*$  relations influence the evolution of channel profiles, focusing on reach slopes and timescales of adjustment. Because the modeling goal is to isolate and understand effects of evolving  $\tau_{c(q_i)}^*$ , the underlying model is arguably the simplest reasonable representation of morphodynamic feedback. Inspired by Parker (2005), the model describes a channel reach in which slope evolves through aggradation and degradation. The downstream boundary elevation is fixed (constant base level). Sediment transport and bed elevation are modeled using Eq. (1) (substituting  $\tau_{c(q_i)}^*$  for  $\tau_c^*$  as needed) and Eq. (7) with a single grain diameter (D). Unit water discharge  $q_w$  is similarly held constant for simplicity. Upstream sediment supply rate  $(q_{sfeed})$  is imposed, and is varied to drive channels to new steady states. Relationships among flow depth, depth-averaged velocity and discharge are imposed by assuming that hydraulic roughness remains constant, parameterized though a Darcy-Weisbach hydraulic friction coefficient:

$$966 f = \frac{8gq_w S}{U^3} \underline{\qquad \qquad (17)}$$

For a given discharge this allows both U and h to be determined:

$$Q68 U = \frac{q_w}{h} \tag{18}$$

$$h = q_w^{2/3} \left(\frac{f}{8gS}\right)^{1/3} \tag{19}$$

Two model variations are compared; in the "Exner-only" morphodynamic model,  $\tau_c^*$ 

is <u>a</u> constant. In the "Exner+ $\tau_{c(q_s)}^*$ " variant,  $\tau_{c(q_s)}^*$  evolves through time following Eq. (10). At

equilibrium, channel slope can be predicted for both model variants (and substituting  $\tau_{c(q_s)}^*$ 

973 for  $\tau_c^*$  where appropriate) by combining Eq. (1), (2), (12) and (19):

$$S_{eq} = \frac{2.83}{q_w} \left(\frac{g}{f}\right)^{1/2} D^{3/2} \left(\frac{\rho_s}{\rho} - 1\right)^{3/2} \left[\left(\frac{q_s^*}{3.97}\right)^{2/3} + \tau_c^*\right]^{3/2}$$
 (20)

Formatted: Font: Not Bold

Deleted:  $\tau_c^*$ 

Formatted: Font: Not Bold

Deleted: evolution

Deleted: <#>Morphodynamic model development¶

Deleted:  $au_s^*$ 

Deleted: reach

Deleted:

Deleted:  $au_c^*$ 

Deleted:

**Deleted:** {Parker, 2005 #4623}

Deleted: G. Parker's Morphodynamics e-book,

Deleted:

Deleted: 4

Formatted: Highlight

Deleted:

**Deleted:** in simulations below

Deleted:

Deleted: 15

Deleted: 16
Deleted: 17

**Deleted:** Although not presented, simulations were also done in which the relation between U and h was determined by instead holding Froude number (  $Fr = U/\sqrt{gh}$  )

constant (Grant, 1997). While f changes systematically with slope in this scenario, resulting trends in reach slope adjustment and response timescales are substantively the same as shown below for constant f, suggesting little sensitivity to the underlying hydraulic closure assumptions.

Deleted:

Deleted: held

Deleted:  $au_c^*$ 

Deleted:  $\tau_c^*$ 

Deleted: 7

Deleted:

Deleted: 9

Formatted: Not Highlight

Deleted: 7

Deleted:

For a given discharge, Eq. (20) indicates that both sediment supply and the threshold of motion influence steady-state morphology (slope).

1011

1012

1013

1014

1015

1016

1017

1018

1019

1020

1021

1022

1023

1024

1025

1026

1027

1028

1029

1030

1031

1032

1033

1034

1035

1036

1037

1038

1039

Deleted: 18

Deleted: change

Away from equilibrium, rates of change of bed elevation along a river profile should depend not only on the sediment flux at a given channel cross section, but also on the average velocity at which grains move downstream. This control has occasionally been ignored in previous models of profile evolution. In my model, it is crudely incorporated by assuming that average bedload velocity is a consistent fraction of water velocity, broadly consistent with previous findings that bedload velocities are proportional to shear velocity (e.g., Martin et al., 2012). The modeling timestep is set to be equal to the time it takes sediment to move from one model node (bed location) to the next, and is adjusted during simulations. While this approach makes the temporal evolution of channel changes internally consistent within the model, timescales for model response will still be much shorter than actual adjustment times in field settings because flood intermittency is not included (so the model as implemented is always at a constant flood discharge). In addition, the upstream sediment supply is imposed in the model, while in natural settings hillslope-floodplain-channel coupling could greatly affect  $q_{sfeed}$  over time if significant aggradation or downcutting took place.

Deleted: morphological

Table 2 provides parameters used for morphodynamic modeling. Although the highly simplified model is not intended for quantitative field comparisons, variables D ( $D_{50}$ =50 mm),  $f_c(0.1)$ , and  $q_w$  (1 m²/s) were chosen to be broadly consistent with a moderate ( $\approx$ 2-3 year peak discharge recurrence interval) bedload-transporting flood in Reynolds Creek, Idaho (Olinde and Johnson, 2015). Reynolds creek is a snowmelt-dominated channel with reach slopes that vary widely from  $\sim$ 0.005 to 0.07. In an instrumented reach with a slope of 0.02, Olinde (2015) used RFID-tagged tracers and channel-spanning RFID antennas to measure  $\tau_{rs50}^*\approx$ 0.06. A constant  $\tau_c^*=0.06$  is used for the Exner-only models, while  $\tau_{c(q_s)}^*=0.06$  is used as the initial condition for Exner+ $\tau_{c(q_s)}^*$  models. Field constraints on upstream sediment feed rates were not available, and so  $q_{sfeed}$  values were chosen to provide reasonable model slopes. Exponents  $\kappa_{dep}$  and  $\kappa_{ent}$  used the experimental calibrations, while k were chosen so that changes in  $\tau_c^*$  occurred over the same range of timescales as topographic adjustments, to better illustrate the interplay of variables in morphodynamic evolution (Table 2).

Deleted:

Deleted:

Deleted:

Deleted:

Deleted:

Deleted: only

Deleted:  $au_c^*$ 

Deleted:  $au_s^*$ 

**Deleted:** with evolving  $au_c^*$ 

Deleted: U

Deleted: (qsfeed)

Deleted: constrained by field data

Deleted: ed

## 3.3.1 Morphodynamic model results

Fig. 6 and 7 compare, how longitudinal profiles respond to an increase in sediments supply, for both the Exner-only (constant  $\tau_c^*$ ) and Exner+ $\tau_{c(q_s)}^*$  models. The initial condition is a channel at equilibrium ( $q_{sout}=q_{sfeed}$ ). At t=0, sediment supply is increased by a factor 5. The Exner+ $\tau_{c(q_s)}^*$  model aggrades to a new equilibrium slope that is lower than the Exner-only model. This occurs because deposition ( $\partial q_s/\partial x < 0$ ) causes  $\tau_{c(q_s)}^*$  to decrease over time, progressively increasing transport efficiency (i.e., higher transport rates at a lower slope) compared to constant  $\tau_c^*=0.06$  (Fig. 7). Feedback causes the reverse effect for a decrease in  $q_{sfeed}$ :  $\tau_{c(q_s)}^*$  progressively increases as slope decreases, leading to channel re-equilibration both sooner and at a higher slope (Fig. 7).

An equilibrium timescale  $(t_{eq})$  is measured <u>here</u> as the amount of time it takes from a supply perturbation (t=0) in these models) to the slope adjusting to be within 0.0001 of its equilibrium slope (Eq. 20). In Fig. 7,  $t_{eq}$  are substantially longer for the Exner-only models than for the Exner+ $\tau^*_{c(q_s)}$  models. For Exner+ $\tau^*_{c(q_s)}$ , an increase in  $q_{sfeed}$  leads to aggradation, in turn increasing local  $q_s^*$  by both increasing slope and also decreasing  $\tau^*_{c(q_s)}$  (Eq. 1, 10). Both factors adjusting enable equilibrium to be reached sooner.

Over a  $q_{sfeed}$  range of two orders of magnitude, equilibrium slopes change less for the Exner+ $\tau_{c(q_s)}^*$  model than for Exner-only (Fig. 8a). The ratio of these equilibrium slopes illustrates the magnitude of the change, where " $S_{eq}$  ratio" is  $S_{eq}$  for Exner+ $\tau_{c(q_s)}^*$  divided by Exner-only  $S_{eq}$  (Fig. 8b). An order-of-magnitude decrease in  $q_{sfeed}$  caused Exner+ $\tau_{c(q_s)}^*$   $S_{eq}$  to be roughly 24% - 36% larger than Exner-only  $S_{eq}$ . An order-of-magnitude increase in  $q_{sfeed}$  caused Exner+ $\tau_{c(q_s)}^*$  to be roughly 20% smaller than the constant- $\tau_c^*$  model. Calculations are also shown for several values of scaling factor k. A larger k means that  $\tau_{c(q_s)}^*$  increases or decreases more rapidly for a given amount of aggradation or degradation (Eq. 10), which in general enables a new equilibrium to be reached with a smaller change in slope.

Deleted:

Deleted: s...how longitudinal profiles respond to an

Formatted: Indent: First line: 0.5'

**Deleted:** having ...he slope adjusting to be within 0.0001

**Deleted:** Fig. 8a confirms, o...ver a q<sub>sfeed</sub> range of two

Formatted: Not Highlight

Deleted: 7

Formatted: Highlight

Equilibrium timescales are quite sensitive to k as well as to sediment supply rate (Fig 8c). Similar to the  $S_{eq}$  ratio, the " $t_{eq}$  ratio" is  $t_{eq}$  for Exner+  $\tau_{c(q_s)}^*$  divided by  $t_{eq}$  for the Exneronly model (Fig. 8d). There is an asymmetry in equilibrium times for aggradation vs. degradation; in general the difference between Exner-only and Exner+  $\tau_{c(q_s)}^*$  is somewhat smaller during bed aggradation, and the difference decreases with increasing  $q_{sfeed}$ . Interestingly, the highest k (2.8E-5) results in a threshold-like response where the  $t_{eq}$  ratio rapidly increases from roughly 0.01 to 0.8 (Fig. 8d). This change occurred because  $\tau_{c(q_s)}^*$  "bottomed out", i.e. reached its minimum possible value ( $\tau_{c(q_s)}^*$   $\tau_{cmin}^*$  =0.02) before the equilibrium slope had been reached (Fig. 8e). At that point,  $\tau_{c(q_s)}^*$  could no longer act as a buffer to reduce slope changes, and it took much longer to reach an equilibrium slope.

Finally, Fig. 9 shows that the spatial as well as temporal evolution of  $\tau_{c(q_s)}^*$  can influence river profiles. The models are the same as in Fig. 6. At t=0, the feed rate into the supstream-most node ( $q_{sfeed}$ ) increases by a factor of 5. Therefore, the upstream end feels the supply perturbation both sooner and more strongly than downstream nodes. Aggradation from the supply perturbation increases upstream slopes first. In the Exner-only model, downstream slopes gradually catch up. Because  $\tau_c^*$  stays constant, every location along the channel eventually asymptotes to the single slope required to transport the new  $q_{sfeed}$  at the given discharge (Fig. 9a). However, for evolving thresholds, enhanced upstream aggradation caused upstream  $\tau_{c(q_s)}^*$  to decrease both more rapidly and to lower values than downstream nodes. Spatial differences in  $\tau_{c(q_s)}^*$  persisted at equilibrium, resulting in spatial variations in equilibrium slope (Exner+  $\tau_{c(q_s)}^*$ ; Fig. 9b, 9c).

## 4 Discussion

In this section, the dependence of  $\underline{\tau_{c(q_s)}^*}$  on sediment supply is compared to previous work.  $\underline{\tau_{c(q_s)}^*}$  evolution is identified as a negative feedback on morphologic change that can impart a memory of previous channel "states" to the system. Finally,  $\underline{\tau_{c(q_s)}^*}$  is interpreted as a channel state variable, analogous to temperature in thermodynamics.

**Deleted:**  $\tau_c^*$  ..., ...  $t_{eq}$  ... ivided by  $t_{eq}$  for the Exner-only

**Deleted:**  $\tau_c^*$ ...can influence river profiles. ...

Formatted ...

Deleted:  $node\ 1,\ 0\ km$ Formatted ...

Deleted: Thus ...herefore, the upstream end feels the flux ...

**Deleted:**  $\tau_c^*$  ... on sediment supply is compared to previo

As described in section 1.1, previous work on sediment supply-dependent thresholds of motion includes Recking (2012), who proposed high sediment supply ( $\tau_{msc}^*$ ; Eq. 5) and low sediment supply ( $\tau_{msc}^*$ ; Eq. 6) bounds on thresholds of motion. Fig. 10 shows how these relations compare to the experimentally-constrained  $\tau_{rs50}^*$ . It should be noted again that these bounds were calibrated to the  $D_{84}$  grain size rather than  $D_{50}$  (Recking, 2012). While the actual values are therefore not expected to be equivalent  $\tau_{mss}^*$  and  $\tau_m^*$  do tend to bound  $\tau_{rs50}^*$ . The low-supply bound  $\tau_m^*$  is roughly 2-4 times larger than the experimental constraints. The high-supply bound  $\tau_{mss}^*$  is similar in magnitude to  $\tau_{rs50}^*$  and predicts the decrease during the feed period. The (linear) correlation between  $\tau_{mss}^*$  and  $\tau_{rs50}^*$  is weak ( $R^2$ =0.13) although statistically significant (p=3E-5). Nonetheless, given that threshold of motion uncertainties are typically large, Eq. (5) arguably provides a surprisingly good independent prediction of our experimental disequilibrium transport data, based on experimental slope,  $D_{84}$  and  $D_{50}$ .

1215

1216

1217

1218

1219

1220

1221

1222

1223

1224

1225

1226

1227

1228

1229

1230

1231

1232

1233

1234

1235

1236

1237

1238

1239

1240

The  $\tau_{c(q_i)}^*$  model is consistent with previous interpretations that high sediment supply-corresponds to low thresholds of motion, and vice-versa (Recking, 2012; Bunte et al., 2013). In the  $\tau_{c(q_i)}^*$  model (Eq. 10), an increase in upstream sediment supply that causes net aggradation will lower  $\tau_{c(q_i)}^*$ , unless  $\tau_{c(q_i)}^*$  has already reached its lower physical limit ( $\tau_{c \min}^*$ ). Conversely, a decrease in supply that causes net erosion will increase  $\tau_{c(q_i)}^*$ , unless  $\tau_{c(q_i)}^*$  is already high ( $\approx \tau_{c \max}^*$ ). However, while the  $\tau_{c(q_i)}^*$  model can thus explain an inverse relation between supply and thresholds of motion, it is worth noting that Eq. (8) and (10) describe a subtly different feedback:  $\tau_{c(q_i)}^*$  does not directly increase or decrease with supply, but rather with the history of sediment supply changes relative to transport capacity over time. If  $q_{sin}$  equals  $q_{sout}$ ,  $\tau_{c(q_i)}^*$  could remain constant regardless of whether  $q_{sin}$  is high or low.

### 4.1 Negative feedback and asymmetric approaches to equilibrium

The evolution of  $\underline{\tau_{c(q_s)}^*}$  acts as a negative feedback because it reduces the morphodynamic response to perturbations. Reach slopes and  $\underline{\tau_{c(q_s)}^*}$  both change in the direction that brings transport back towards equilibrium, allowing smaller slope changes to

Deleted: <#>Comparison to previous work¶ Formatted: Indent: First line: 0.5' Deleted: Deleted: compared long-term bed load monitoring record **Deleted:** reference stresses parameters **Deleted:** describe transport of Deleted: ( Deleted: ) using a different transport model **Deleted:** Nonetheless,  $au_{mss}^*$  and  $au_m^*$  were shown to be Deleted: Deleted: low Deleted: 3 Deleted: Deleted: While Deleted: , t Deleted: Deleted: 19 Deleted: Deleted: ¶ Formatted: Indent: First line: 0.49" Formatted: Not Highlight Deleted: W Deleted:  $\tau_c^*$ **Deleted:** -evolution Deleted: is **Deleted:** not inconsistent with high sediment supply rates Deleted: 5 Deleted: 7 Deleted: say Deleted: something Deleted: different Deleted:  $\tau_c^*$ Deleted:  $\tau_c^*$ Deleted: will Deleted: Formatted: Font: Not Bold

Deleted:  $\tau^*$ 

Deleted:  $\tau_a^*$ 

accomodate supply changes (Fig. 6, 7, 8a,b, 9). However, as with other buffered systems, there is a limit to how large of a perturbation can be accommodated by  $\underline{\tau}_{c(q_i)}^*$  (as illustrated by k=2.8E-5 in Fig. 8c,d,e). The amount of possible  $\underline{\tau}_{c(q_s)}^*$  change depends on how close  $\underline{\tau}_{c(q_s)}^*$  is to  $\underline{\tau}_{c\min}^*$  or  $\underline{\tau}_{c\max}^*$  (Eq. 9). When changes in  $\underline{\tau}_{c(q_s)}^*$  are <u>negligible</u> but transport and morphology are not equilibrated, then the time to equilibrium ( $t_{eq}$ ) increases because only channel morphology can adjust (Fig. 8c, d, e).

1305

1306

1307

1308

1309

1310

1311

1312

1313

1314

1315

1316

1817

1318

1319

1320

1321

1322

1323

1324

1325

1326

1327

1328

1329

1330

1331

1332

The experiments suggest that  $au_{c(q_s)}^*$  changes faster in response to aggradation than degradation (Fig. 2, 5). This asymmetry is expressed in the best-fit exponents:  $\kappa_{dep}$  is smaller than  $\kappa_{ent}$  for all scenarios tested (Table 1). Note that because  $\partial \theta_s/\partial x$  is much smaller than 1 (i.e, spatial changes in bed elevation are small compared to the horizontal distance the change is measured over), the smaller exponent ( $\kappa_{dep}$ ) corresponds to a larger change in  $\tau_{c(q_i)}^*$  for a given  $\partial \theta_s/\partial x$  (Eq. <u>10</u>). For a given increment of sediment thickness ( $\theta_s$ ), aggradation is more efficient at decreasing  $\tau_{c(q_i)}^*$  than degradation is at increasing  $\tau_{c(q_i)}^*$ . Future work is required to explore how specific physical processes vary during net deposition or erosion and <u>lead to asymmetry in  $\tau_{c(q_i)}^*$  change. Still, a tentative hypothesis linking bed roughness and</u>  $\tau_{c(q_s)}^*$  change asymmetry is that during deposition, clasts tend to deposit preferentially in topographic lows, because these tend to be the most sheltered locations, and simply because of the direction of gravity. Preferentially filling in lows tends to decrease bed roughness, in turn reducing topographic sheltering and hydraulic friction and increasing near-bed flow velocities. All of these factors decrease  $\tau_{c(q_s)}^*$ . However, erosion does not simply have an opposite but symmetric effect on bed topography as deposition. Clasts are not preferentially eroded from topographic lows, as these locations tend to remain the most sheltered. Instead, the process of increasing bed roughness during erosion is more complex and results from the more gradual development of stabilizing structures around keystones, as grains are rearranged locally to positions where they protrude into the flow but remain stable due to interlocking with surrounding grains. Thus, roughness reduction and enhancement should not equally sensitive to net erosion or deposition. Mao (2012) showed that bed roughness evolved at different rates during symmetric rising and falling limbs of hydrographs, influencing gravel

Deleted: $ au_c^*$
Deleted:
Deleted: $ au_c^*$
Deleted: the
Deleted: $ au_c^*$
<b>Deleted:</b> the threshold boundaries, i.e.
Deleted: 5, 7
Deleted: $ au_c^*$
<b>Deleted:</b> no longer possible (or are asymptotically small
Deleted: )
Deleted: $ au_c^*$
Deleted:
Deleted: $ au_c^*$
Deleted: 7
Deleted:
Deleted: Thus

**Deleted:** , for a given increment of sediment thickness (  $\theta_{\rm c}$  )

Deleted:  $\tau$ 

Deleted:  $\tau_c^*$ 

transport hysteresis. Bed roughness due to sand ripple and dune evolution has also been shown to increase and decrease at different rates during hydrograph rising and falling limbs, leading to hysteresis in a transport system that is not threshold dominated (Martin and Jerolmack, 2013).

1352

1353

1354

1355

1356

1357

1358

1359

1360

1361

1362

1363

1364

1365

1366

1367

1368

1369

1370

1371

1372

1373

1374

1375

1376

1377

1378

1379

In Fig. 8c, the Exner+ $\tau^*_{c(q_s)}$  model indicates that equilibrium timescales are longer for aggradation ( $q_{sfeed}$  / initial  $q_{sfeed} > 1$ ) than for degradation. At first glance this seems to contradict the argument that aggradation is more efficient at decreasing  $\tau^*_{c(q_s)}$ . The explanation is that the equilibrium timescale does not *only* depend on the exponents, but also on how much total aggradation or degradation occurs to attain equilibrium. Slope changed more during aggradation than degradation for these particular Exner+ $\tau^*_{c(q_s)}$  models, even though  $\tau^*_{c(q_s)}$  also tended to change more during aggradation than degradation (Fig. 8a. 8e).

In the experiments, average slopes changed very little in response to changes in sediment supply and transport disequilibrium, while grain size and bed surface roughness changed much more (Fig. 2; bed roughness is presented in detail in Johnson et al., 2015). Because the W&CM accounted for surface grain size changes in determining experimental  $\tau_{rs50}^*$  (Fig. 3), bed roughness and various unquantified mechanisms (such as grain interlocking) are interpreted to have physically caused the  $\tau_{rs50}^*$  evolution. What does this suggest for k, which scales how much  $\tau_{c(q_i)}^*$  changes for a given amount of aggradation or degradation? The best-fit k was 2.83E-3 s<sup>-1</sup>, which reflects the rapid adjustment of experimental  $\tau_{c(q_i)}^*$  compared to slope changes (Fig. 5, Table 1, Eq 10). In contrast, the morphodynamic modeling used k values adjusted to be 2 to 3 orders of magnitude smaller, so that the response to a perturbation in supply would involve non-negligible changes in slope (the only morphologic variable in the simple morphodynamic model) as well as in  $\tau_{c(q_i)}^*$ . Higher values of k in the morphodynamic model cause  $\tau_{c(q_i)}^*$  to adjust more rapidly and slope to adjust less (Fig. 8).

An implication of  $\tau_{c(q_s)}^*$  evolving with reach morphodynamics is that local channel form can retain "memories" of previous conditions, which can influence local responses to subsequent forcing In Fig. 9b and 9c, an increase in supply led to the temporal and spatial

Deleted: But why then does Deleted: indicate Deleted: for t Deleted:  $\tau_a^*$ Deleted: Deleted: ? Deleted: , and how quickly sediment enters or exits the reach to enable that aggradation or degradation Deleted: More s Deleted: occurred Deleted:  $\tau_a^*$ Deleted: (Fig. 8a) Deleted:  $\tau_c^*$ Deleted: by Deleted: (Fig. 2) **Deleted:** were accounted for (by the W&CM) Deleted: (presented in detail in Johnson et al., 2015) Deleted: other Deleted: Deleted:  $\tau$ **Deleted:** to the collective experiments Deleted:  $\tau$ Formatted: Not Highlight Deleted: 7 Formatted: Highlight Deleted: Deleted:  $\tau_c^*$ Deleted: Deleted:  $\tau_c^*$ Deleted:

Deleted: <#>Memory, morphologic variability, and

Reynolds Creek¶

Deleted:  $au_c^*$ 

evolution of  $\tau_{c(q_s)}^*$ , which in turn caused spatial variations in equilibrium slope. Upstream reaches acted as filters of the supply perturbation to downstream reaches. In nature, spatially and temporally-averaged morphodynamic equilibrium will reflect "channel-forming" discharges and a representative sediment supply from upstream, but floods, local supply perturbations and history add to spatial variability in both  $\tau_{c(q_s)}^*$  and morphology. I also acknowledge that the model parameters were calibrated to flume experiments at steep 8% and 12% slopes with a GSD that includes scaled boulders (Table 1; Johnson et al., 2015); future work is required to determine how the surface GSD influences the strength of  $\tau_{c(q_s)}^*$  evolution, and how well the model predicts  $\tau_{c(q_s)}^*$  changes in lower slope gravel-bed rivers.

## 4.2 State variable framework for modeling morphodynamics

1412

1413

1414

1415

1416

1417

1418

1419

1420

1421

1422

1423

1424

1425

1426

1427

1428

1429

1430

1431

1432

1433

1434

1435

1436

1437

1438

1439

1440

Next, I argue that  $\tau_{c(q_i)}^*$  should be redefined as a state variable (or state function) for gravel-bed channels, and outline a possible state variable approach for modeling the morphodynamic evolution of channels. The term "bed state" has long been informally used to describe collective aspects of local channel morphology, such as surface GSD and armoring and clustering, that change with relative ease and influence transport rates (e.g., Church, 2006; Gomez and Church, 1989). Although explicitly defining  $\tau_{c(q_i)}^*$  evolution and related feedbacks in terms of state and path variables appears to be novel (to my knowledge), channel morphodynamics have long been implicitly described using similar ideas. For example, Phillips (2007) presented a qualitative conceptual model of Jandscape evolution in terms of improbable system states arguing that although deterministic process "laws" act on topography, the actual outcome (i.e., any particular landscape) depends on initial conditions and in particular is sensitive to history, Many other works have similarly generalized complex channel process and response feedbacks to understand morphodynamics (e.g., Fonstad, 2003; Phillips, 2011, 2009; Chin and Phillips, 2007; Phillips, 1991; Stark and Stark, 2001; Yanites and Tucker, 2010).

State variables are integral to many disciplines, including control systems engineering and thermodynamics. Thermodynamic state variables include temperature, pressure, enthalpy and entropy. By definition state variables are path-independent (Oxtoby et al., 2015). For example, temperature (*T*) describes the amount of thermal energy per unit of a material. A

Deleted:  $\tau_s^*$ Deleted: Deleted: (here, "reach" refers to a small fraction of the total modeled longitudinal distance) Deleted: In contrast, slope variability developed during the transient adjustment period when  $\tau_a^*$  remained constant, but all reaches evolved to the same equilibrium slope required to transport the new supply (Fig. 9a). ¶ Natural river channels inevitably exhibit morphologic variability at reach scales. For example, although the longitudinal profile of Reynolds Creek appears smoothly concave over a spatial scale of 10 km (Fig. 11a), there is substantial slope variability when calculated for 100 m reaches (Fig. 11b). This 100 m averaging scale was chosen for the following analysis because it is sufficiently large to plausibly be used for landscape evolution modeling, while small enough to capture slope variability along a profile. Deleted: local Deleted:  $\tau_c^*$ Deleted: function Formatted: Font: Not Bold Deleted:  $\tau$ Deleted: is an important Deleted: function Deleted: **Deleted:** describing  $\tau$ Deleted: river **Deleted:** function Deleted: may Deleted: t Deleted: Phillips (2007) Deleted: his approach is in many ways conceptually Deleted: and form Deleted: and the importance of history Deleted: **Deleted:** and similar to **Deleted:** that describe and **Deleted:** morphology

**Deleted:** or state functions

**Deleted:** are some of the many thermodynamic state

Deleted: For example,

change in temperature depends only on the initial and final states (i.e.,  $\Delta T = T_2 - T_1$ ), but does not depend on the path, i.e. the history of temperatures between times  $t_2$  and  $t_1$ . In contrast, heat—the flow (transfer) of thermal energy—is a path variable (or process variable), not a state variable. Heat flow between bodies is both controlled by and changes the temperature of those bodies, but the amount of total heat transferred does depend on the path. Three other points about state variables are relevant to morphodynamics. First, state variables are variables are variables are relevant to morphodynamics. First, state variable calculated from temperature, enthalpy and entropy (Hemond and Fechner, 2014). Second, although state variables are technically only defined at equilibrium, in practice they are useful for understanding gradually evolving systems (e.g., Kleidon, 2010). Third, the evolution of systems involving multiple state variables are usually described with coupled differential equations.

Channel morphodynamics <u>can</u> be described by a similar framework of state and path <u>variables</u>. Analogous to heat, the cumulative discharges of both water and sediment are path <u>variables</u> that drive bed state evolution. Channel morphology can be described by numerous bed state variables, including but not limited to surface GSD, slope, width, depth, bed roughness, surface grain clustering, interlocking, overlap and imbrication, and finally  $\tau_{c(q_1)}^*$ .

Analogous to temperature, I explicitly define  $\tau_{c(q_1)}^*$  as a state variable. The amount of change change in  $\tau_{c(q_1)}^*$  from time  $t_1$  to  $t_2$  does not depend on the progression of values in between. However, the amount of sediment transported between  $t_1$  and  $t_2$  does depend on the history of  $\tau_{c(q_1)}^*$ , and also influences the history of  $\tau_{c(q_1)}^*$  (Eq. 8, 10).

Entropy is the state variable perhaps used most often to characterize channel systems (e.g., Chin and Phillips, 2007; Leopold and Langbein, 1962; Rodriguez-Iturbe and Rinaldo, 1997). Entropy can provide a closure for underconstrained sets of equations, by assuming that geomorphic systems inherently maximize their entropy at equilibrium (Kleidon, 2010; Chiu, 1987). A limitation of some maximum-entropy landscape models is that physically-based surface processes are not always explicitly modeled, making them less useful for predicting landscape responses to environmental perturbations, even if they can create reasonable equilibrium morphologies (Paik and Kumar, 2010). In contrast to entropy, state variable  $\tau_{c(q_i)}^*$  has a clear process-based meaning.

**Deleted:** of the material ...epends only on its ...he initial

**Deleted:** traditional ...tate functions ...ariables are

Deleted:

**Deleted:** could ...an be described by a similar framework

Formatted: Highlight

**Deleted:** It is worth noting that e

**Deleted:** is often used to...an provide a closure for

**Deleted:** results difficult to validate and...hem less useful

**Deleted:** function ariable  $\tau^*$ ,  $\tau^*$ 

I suggest that landscape evolution models could incorporate subgrid-scale channel feedbacks by treating  $\tau_{c(q_s)}^*$  as a state variable. Conceptually, the  $\tau_{c(q_s)}^*$  model "lumps" processes related to multiple bed state variables (sections 1.1, 2.1). Similarly, because many channel state variables influence transport and therefore are not independent of  $\tau_{c(q_s)}^*$ . I hypothesize that aspects of morphology can be implicitly subsumed into evolving  $\tau_{c(q_s)}^*$  for modeling purposes, because  $\tau_{c(q_s)}^*$  captures essential feedbacks over spatial and temporal scales of interest. This is similar to the channelization approach of Stark and Stark (2001).

## 4.3 Form drag vs. parsimony

1626

1627

1628

1629

1630

1631

1632

1633

1634

1635

1636

1637

1638

1639

1640

1641

1642

1643

1644

1645

1646

1647

1648

1649

1650

1651

1652

Calculations of best-fit  $\tau_{rs50}^*$  and transport rates used total shear stress (Eq. <u>12</u>), rather than partitioning stress into form drag and a lower effective stress for calculating transport rates (skin friction). Although not a state variable, form drag is physically justifiable because larger clasts that protrude higher into the flow (e.g. stable boulders) tend to account for a disproportionate amount of the total stress through drag, turbulence generation and pressure gradients. Form drag corrections have been incorporated into many transport models to enable reasonable transport rates to be calculated using  $\tau_c^*$  values typical of systems without form drag (e.g., Rickenmann and Recking, 2011; David et al., 2011; Yager et al., 2012a). Conversely, another common approach (and that taken here) is simply to use higher  $\tau_c^*$  (e.g., Bunte et al., 2013; Lenzi et al., 2006), consistent with acknowledging that  $\tau_c^*$  can be a physically meaningful fitting parameter to predict transport. Using field data, Schneider et al. (2015) recently compared gravel transport predictions based on (a) form drag corrections and (b) higher reference stresses. For the most part, they found that both approaches could provide similar accuracy. They also noted that "uncertainties in predicted transport rates remain huge (up to roughly 3 orders of magnitude)" (Schneider et al., 2015), and suggested that factors including supply effects may account for remaining discrepancies. Although beyond the scope of the present analysis, form drag effects could be separated from best-fit  $\tau_{rs50}^*$  by using a calculated skin friction stress rather than total stress. However, doing so would add extra uncertainty to the shear stresses, while still not directly accounting for effects of sediment **Deleted:** How could a state function framework improve morphodynamic modeling and incorporate subgrid-scale channel feedbacks into broader landscape evolution models? Simplicity is important: the most insight is often gained by using the simplest possible model that can still capture essential feedbacks over spatial and temporal scales of interest. As described in the introduction, previous work has shown that  $\tau_c^*$  is influenced by many characteristics of the surrounding bed surface.

**Deleted:** In other words,  $\tau_c^*$ 

Deleted: is closely

Deleted: other

Formatted: Font: Italic

Deleted:

**Deleted:** It would probably be impractical to develop or apply a "complete"  $\tau_c^*$  model that explicitly incorporated separate state variables for multiple known controls on  $\tau_c^*$ .

Instead, the  $\tau_c^*$  evolution equation (Eq. 5, 7) attempts to strike a balance between predicting process in a physically justifiable (but empirically calibrated) way, while remaining broadly applicable. It could similarly be impractical to apply a "complete" reach-scale morphodynamic model that explicitly parameterized myriad feedbacks using every corresponding bed state variable. Instead

Deleted: bed

Formatted: Font: Italic

Deleted: actually

Deleted:  $\tau_c^*$ 

Deleted:  $au_c^*$ 

**Deleted:** For example, in the {Johnson, 2015 #4610@@author-year}experiments the bed responded to transport disequilibrium primarily by changing roughness but not slope. However, roughness was not an explicit, separate variable in the best-fit  $\tau_{rs50}^*$  calculations. Instead, some effects of evolving roughness and other bed state controls (imbrication, clustering) on transport rates became implicitly accounted for in the experimentally calibrated  $\tau_{rs50}^*$  ( $\approx \tau_c^*$ ). The best-fit model parameters  $(k, \kappa_{dep}, \tau_{ep})$ 

 $K_{ent}$ ; Eq. 7; Table 1) would presumably change if a separate differential equation was developed to explicitly

Formatted: Font: Not Bold

Deleted: 9

Deleted: used

Deleted: on steep channel gravel transport

Deleted: either

supply. Implicitly subsuming form drag into  $\tau_{c(q_i)}^*$  arguably provides a simpler and more parsimonious approach for modeling transport and morphodynamics.

5 Conclusions

I propose a new model in which feedback causes  $\tau_{c(q_i)}^*$ , the nondimensional critical shear stress for gravel transport, to evolve through time as a function of sediment transport

stress for gravel transport, to evolve through time as a function of sediment transport disequilibrium (Eq. 8, 10). Net erosion tends to increase local  $\tau_{c(q_i)}^*$  (reducing transport rates), while net deposition tends to decrease  $\tau_{c(q_i)}^*$  (increasing transport rates). Laboratory flume experiments described by Johnson et al. (2015) are used to evaluate the proposed  $\tau_{c(q_i)}^*$  model. The experiments intentionally explored disequilibrium bedload transport and morphodynamic adjustment. Thresholds of motion were back-calculated from the experimental data using the Wilcock and Crowe (2003) model for mixed grain size transport. It also show that the Wilcock and Crowe (2003) hiding function is consistent with our experimental data, supporting its applicability to steep channels.

After empirically <u>calibrating</u> three model parameters, the  $\tau_{c(q_s)}^*$  model—a differential equation—can explain nearly 70% of the variability in experimental <u>thresholds of motion.</u> I then incorporate  $\tau_{c(q_s)}^*$  into a simple <u>morphodynamic</u> model for channel <u>profile</u> evolution. Changes in  $\tau_{c(q_s)}^*$  are negative feedbacks on morphodynamic response, because not only slope but also  $\tau_{c(q_s)}^*$  evolve when perturbed.

Finally,  $\tau_{c(q_i)}^*$  is <u>redefined</u> to be a state variable for fluvial channels. State functions and path functions are fundamental to many disciplines such as thermodynamics, because they allow the evolution of systems to be calculated. The same should be true for <u>morphodynamics</u>. Conceptualizing Jandscape evolution models in terms <u>of</u> feedbacks among evolving state variables and path functions may improve our ability to predict landscape responses to land use, climate change and tectonic forcing.

Acknowledgements

1713

1714

1715

1716

1717

1718

1719

1720

1721

1722

1723

1724

1725

1726

1727

1728

1729

1730

1731

1732

1733

1734

1735

1736

1737

Deleted:  $\tau_c^*$ Deleted: Flume data and a corresponding model demonstrate that nondimensional critical shear stress ( $\tau_c^*$ ) Deleted: s Formatted: Not Highlight Deleted:  $\tau_c^*$ Deleted:  $\tau$ **Deleted:** This  $\tau_c^*$  dependence on sediment supply relative to transport capacity can plausibly explain much of the ~order-of-magnitude variability almost inevitably observed in transport threshold data (Fig. 1). This view contrasts wit **Deleted:** Flume experiments measured sediment transpor Deleted: , to back-calculate both hiding function exponen Deleted: T Deleted: provides a good prediction of our **Deleted:** (including different exponents for relatively sm **Deleted:** A new differential equation is proposed for Deleted: fitting Deleted: is **Deleted:**  $\tau_c^*$ -evolution Deleted: Deleted:  $\tau_c^*$ . Deleted: We **Deleted:** the  $\tau_c^*$ -evolution equation Deleted: slope Deleted:  $\tau_c^*$ Deleted:  $\tau_c^*$ Deleted: **Deleted:** Evolving  $\tau_c^*$  also reduces response timescales,

Deleted:  $\tau$ 

Deleted:

Deleted:

Deleted: interpreted

Deleted: More broadly, c

Deleted: morphodynamic and

**Deleted:** channels; sediment transport is to heat as  $\tau_c^*$  is  $\tau$ 

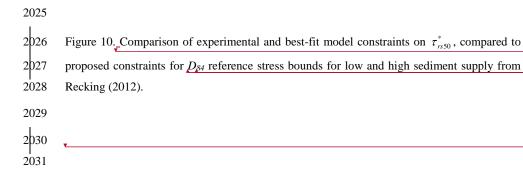
1808	I thank Alex	Aronovitz for conducting the flume experiments, Wonsuck, Kim for aiding in the	_	Deleted: .
1809	experimental	design, Lindsay Olinde for helpful discussions, and Mike Lamb and Jeff	_	Deleted: .
1810	Prancevic for	sharing their $\tau_c^*$ compilation. J also thank Jens Turowski, two anonymous	1	Deleted: .
				<b>Deleted:</b> Reynolds Creek analysis and
1811		AE Daniel Parsons for constructive feedback. Support came from NSF grant	$/\!/$	Deleted:
1812	EAR-105350	8.	$\  \ \  $	Deleted:
1813				Deleted: data
.h.,				Deleted:  Deleted: the kind-hearted reviewers and editor.
1814	Appendix 1	List of variables	_ \	Deleted: the kind-hearted reviewers and editor.
1815	$A_{r_{\bullet}}$	Dimensionless parameter for incorporating grain size or roughness ratios in		Deleted:
1816	, <u>-</u>	Eq. (10) [1]	_	Deleted:
1510		Eq. (10) [1]		Deleted: 7
1817	b	Dimensionless hiding function exponent; either described by Eq. (16) or fit as		Deleted: 13
1818		a single value [1]		
1810	D	Dimensional "for all als for 4". For (0) [1]		
1819	В	Dimensionless "feedback factor"; Eq. (9)[1]		Deleted: 6
1820	$c_1, c_2, c_3$	Dimensionless empirical constants in Eq. (4) [1]		Deleted: 1
1821	D	Grain diameter, for model cases with a single size only [L]		
1822	$D_{50}$	Median grain diameter [L]		
1823	$D_{s50}$	Median grain diameter of bed surface [L]		
1824	$D_i$	Grain diameter of size class <i>i</i> [L]		
1005	C	D. W. I. I. I. I. C. C		
1825	f	Darcy-Weisbach hydraulic friction coefficient; Eq. (17) [1]		Deleted: 5
1826	Fr	Froude number [1]		
1827	$F_{i}$	Areal fraction of grain size class $i$ on the bed surface; Eq. 1 $\frac{3}{2}$ [1]	/	Deleted: 0
1828	$F_s$	Areal fraction of sand on the bed surface; Eq. 4 [1]		Deleted: 1
1829	g	Gravitational acceleration [LT <sup>-2</sup> ]		
1830	h	Water depth [L]		
1831	$K_{dep}$	Exponent for net deposition in $\tau_c^*$ -evolution models; Eq. (8), (10). [1]		Deleted: 5
	ucp		_	Deleted: 7
1832	$K_{ent}$	Exponent for net erosion in $\tau_c^*$ -evolution models; Eq. (8), (10). [1]		Deleted: 5
I			_	Deleted: 7

1856	k	Scaling factor for $\tau_c^*$ evolution. Dimensions are [1/T] for Eq. (10)		Deleted: 7
1857	$\lambda_{_{P}}$	Bed porosity [1]		
1858	$q_{\it bi}$	Volume sediment flux per unit width of size class i in Wilcock and Crowe		
1859		(2003); Eq. 1 <u>3</u> [L <sup>2</sup> /T]	(	Deleted: 0
1860	$q_s$	Volume sediment flux per unit width [L <sup>2</sup> /T]		
1861	$q_s^*$	Nondimensional volume sediment flux; Eq. (1) [1]		
1862	$q_{ m sin}$	Sediment flux entering a channel bed area (reach) of interest $[L^2/T]$		
1863	$q_{sout}$	Sediment flux exiting a channel bed area (reach) of interest [L <sup>2</sup> /T]		
1864	$q_{\it sfeed}$	Sediment flux entering upstream end of overall model domain $[L^2/T]$		
1865	$q_{\scriptscriptstyle w}$	Volume water discharge per unit width [L <sup>2</sup> /T]		
1866	ρ	Water density [M/L <sup>3</sup> ]		
1867	$ ho_s$	Sediment density [M/L <sup>3</sup> ]		
1868	S	Water surface slope [1]		
1869	$S_{\it eq}$	Water surface slope when reach is at equilibrium [1]		
1870	$\sigma$	Bed roughness, measured here as the standard deviation of detrended bed		
1871		elevations [L]		
1872	$ heta_{s}$	Thickness of sediment deposited or eroded in a time interval; Eq. (10) [L]	(	Deleted: 7
1873	t	Time [T]		
1874	$t_{eq}$	Equilibrium timescale for morphological adjustment [T]		
1875	τ	Shear stress; Eq. (3), (12) [MT <sup>-2</sup> L <sup>-1</sup> ]		
1876	$ au^*$	Shields stress (nondimensional shear stress) [1]		
1877	$ au_c^*$	Critical Shields stress (nondimensional critical shear stress); Eq. (1) [1]		
1878	$ au_{c(q_s)}^*$	Critical Shields stress in new threshold evolution model; Eq. (8), (10) [1]		

1882	$ au_{c ext{max}}^*$	Imposed maximum bound for $\tau_{c(q_s)}^*$ in Eq. (9) [1]		Deleted: $ au_c^*$
1002	*	T		Deleted: 5
1883	$ au_{c ext{min}}^*$	Imposed minimum bound for $\tau_{c(q_i)}^*$ in Eq. (9) [1]	_ `	Deleted: , (7)
1884	$ au_{mss}^*$	High sediment supply nondimensional reference stress end-member bound in		Deleted: $ au_c^*$
1885		Recking (2012) transport model; Eq. (5) [1]		Deleted: 5
1503		recking (2012) transport model, Eq. (3/11)		Deleted: , (7)
1886	${ au}_m^*$	Low sediment supply nondimensional reference stress end-member bound in		Deleted: 19
1887		(Recking, 2012) transport model; Eq. (6) [1]		Deleted: 20
1888	$ au_{\it ri}^*$	Reference Shields stress for size class $i$ , from Wilcock and Crowe (2003) (Eq.		
1889		<u>15)</u> [1]		
1890	$ au_{rm}^*$	Reference Shields stress for geometric mean surface diameter, Eq. (4) [1]		
1891	$ au_{rs50}^*$	Nondimensional reference Shields stress for surface grains of size $D_{s50}$ . Eq. $\leftarrow$		Formatted: Indent: Left: 0", Hanging: 0.98"
1892		<u>(15)</u> [1]		
1893	U	Depth-averaged water velocity, Eq. (17), (18) [L]		
1894	$u_{\tau}$	Shear velocity; Eq. (13) [L/T]		Deleted: 0
	$u_{\tau}$	Shear velocity; Eq. (13) [L/T]  Position measured horizontally (distance along channel) [L]	/	Deleted: 0
1894				Deleted: 0
1894 1895	x	Position measured horizontally (distance along channel) [L]		Deleted: 0
1894 1895 1896	x z	Position measured horizontally (distance along channel) [L]  Position measured vertically (bed elevation)[L]		Deleted: 0
1894 1895 1896 1897	x z	Position measured horizontally (distance along channel) [L]  Position measured vertically (bed elevation)[L]  Nondimensional bedload transport rate for grain size class $i$ , in Wilcock and		Deleted: 0
1894 1895 1896 1897 1898	$x$ $z$ $W_i^*$	Position measured horizontally (distance along channel) [L]  Position measured vertically (bed elevation)[L]  Nondimensional bedload transport rate for grain size class <i>i</i> , in Wilcock and Crowe (2003), Eq. (13), (14) [1]		Deleted: 0
1894 1895 1896 1897 1898 1899	$x$ $z$ $W_i^*$	Position measured horizontally (distance along channel) [L]  Position measured vertically (bed elevation)[L]  Nondimensional bedload transport rate for grain size class <i>i</i> , in Wilcock and Crowe (2003), Eq. (13), (14) [1]		Deleted: 0
1894 1895 1896 1897 1898 1899 1900	$x$ $z$ $W_i^*$ W&CM  Captions	Position measured horizontally (distance along channel) [L]  Position measured vertically (bed elevation)[L]  Nondimensional bedload transport rate for grain size class <i>i</i> , in Wilcock and Crowe (2003), Eq. (13), (14) [1]		Deleted: 0  Deleted:
1894 1895 1896 1897 1898 1899 1900 1901 1902	$x$ $z$ $W_i^*$ W&CM  Captions  Figure 1 The	Position measured horizontally (distance along channel) [L]  Position measured vertically (bed elevation)[L]  Nondimensional bedload transport rate for grain size class <i>i</i> , in Wilcock and Crowe (2003), Eq. (13), (14) [1]  Abbreviation for Wilcock and Crowe (2003) transport model.		
1894 1895 1896 1897 1898 1899 1900	$x$ $z$ $W_i^*$ W&CM  Captions  Figure 1. The regression to	Position measured horizontally (distance along channel) [L]  Position measured vertically (bed elevation)[L]  Nondimensional bedload transport rate for grain size class <i>i</i> , in Wilcock and Crowe (2003), Eq. (13), (14) [1]  Abbreviation for Wilcock and Crowe (2003) transport model.		Deleted:
1894 1895 1896 1897 1898 1899 1900 1901 1902 1903 1904	$x$ $z$ $W_i^*$ W&CM  Captions  Figure 1. The regression to explained by	Position measured horizontally (distance along channel) [L]  Position measured vertically (bed elevation)[L]  Nondimensional bedload transport rate for grain size class $i$ , in Wilcock and Crowe (2003), Eq. (13), (14) [1]  Abbreviation for Wilcock and Crowe (2003) transport model.  reshold of motion data from both field and experimental studies. A power law these data gives $R^2$ =0.34, indicating that a majority of the variability is not slope alone. Dotted lines indicate common range of $\tau_c^*$ =0.03 to 0.06 often		Deleted: Deleted:
1894 1895 1896 1897 1898 1899 1900 1901 1902 1903 1904 1905	$x$ $z$ $W_i^*$ W&CM  Captions  Figure 1 The regression to explained by assumed for the second control of th	Position measured horizontally (distance along channel) [L]  Position measured vertically (bed elevation)[L]  Nondimensional bedload transport rate for grain size class $i$ , in Wilcock and Crowe (2003), Eq. (13), (14) [1]  Abbreviation for Wilcock and Crowe (2003) transport model.  reshold of motion data from both field and experimental studies. A power law these data gives $R^2$ =0.34, indicating that a majority of the variability is not slope alone. Dotted lines indicate common range of $\tau_c^*$ =0.03 to 0.06 often modeling transport, although measured data fall well out of this range. Data have		Deleted:
1894 1895 1896 1897 1898 1899 1900 1901 1902 1903 1904	$x$ $z$ $W_i^*$ W&CM  Captions  Figure 1. The regression to explained by assumed for a been addition	Position measured horizontally (distance along channel) [L]  Position measured vertically (bed elevation)[L]  Nondimensional bedload transport rate for grain size class $i$ , in Wilcock and Crowe (2003), Eq. (13), (14) [1]  Abbreviation for Wilcock and Crowe (2003) transport model.  reshold of motion data from both field and experimental studies. A power law these data gives $R^2$ =0.34, indicating that a majority of the variability is not slope alone. Dotted lines indicate common range of $\tau_c^*$ =0.03 to 0.06 often		Deleted: Deleted:

1021	D 65 - 114 - (1997) - 11 - 114 - 1 - 011 - (2015) - 11 - 114 - 1		
1921	Buffington and Montgomery (1997), with additional data from Olinde (2015) and Lenzi et al.		
1922	(2006),		Deleted:
1923			
1924	Figure 2. Flume experiment data (Johnson et al., 2015), a. Sediment transport rate in ( $Q_{sfeed}$ )		Deleted:
1925	and out of the flume. The upstream sediment supply rate was zero other than during the $Q_{sfeed}$		Deleted:
1926	period. Experiment 1 was run for a longer duration than the others but shows similar trends.		
1927	Note that the outlet $Q_s$ adjusts much faster to match the increase in supply than it does to		
1928	decrease during periods of no input, b. Median bed surface grain diameters decreased during		Deleted:
1929	the feed of finer gravel, and then increase beyond their previous stable bed_c. Flume-averaged		Deleted:
1930	bed slopes changed relatively little even as transport rates and $D_{50}$ changed greatly in response		
1931	to initial bed stabilizing and supply perturbations.		
1932			
1	*		
1933	Figure 3. $\tau_{rs50}^*$ fits to the experimental data with the W&CM. "W&CM fit" uses Eq. (16) to	<	Deleted: 3
1934	calculate hiding function exponent b, while "Power-law fit" calculates a best-fit b along with		Deleted: 5
1935	$\tau_{rs50}^*$ Error bars give 95% confidence intervals on $\tau_{rs50}^*$ based on the regressions; although		Deleted:
1936	uncertainty can be broad the trends are clear and consistent. Shaded area indicates times of		Deleted:
1937	fine gravel addition (sediment feed) in each experiment		Deleted:
1938			
Ī	Fig. 4 D		
1939	Figure 4. Data points are based on power-law fits to exponent <u>b</u> . The W&CM hiding function		Formatted: Font: Italic
1940	(Eq. 16) does a good job matching the data, although it was not fit to these points. The first 6	<	Deleted: 3  Deleted:
1941	measurements of each experiment (roughly the first 10 minutes) were excluded because of		
1942	large scatter associated with the greatest bed instability. The axes reflect the left and right	<	Deleted:
1943	hand sides of Eq. (15), but uses dimensional stresses to be consistent with plots shown in	_	Deleted: 2
1944	Wilcock and Crowe (2003).		Deleted: although the plot
1945			
1946	Figure 5 Best-fit models (Eq. 4, 8 and 10) compared to experimental constraints. The periods		Deleted:
1947	of upstream sediment supply ( $Q_{sfeed}$ ) are indicated by the grey boxes for each experiment.		Deleted: 7 and
		\	Believed 4

1968	Figure 6 Profile evolution, comparing the morphodynamic responses of models with and	Deleted:
1969	without threshold evolution. The initial condition is an equilibrium channel with $\tau_{c(q_i)}^*=0.06$ ,	Deleted:
1970		Deleted: $ au_c^*$
	upstream sediment supply $q_s$ =1e-3 m <sup>2</sup> /s, and an initial equilibrium slope of 0.0147. Sediment	Deleted:
1971	supply is increased 5x at #=0.*Lines are each 5 model days apart, and indicate the evolution to	Formatted: Font: Italic
1972	a new transport equilibrium.▼	Deleted:
1973		Deleted:
1974	Figure 7. Slope and critical shear stress evolution, for sediment supply increases (which	Deleted:
1975	correspond to Fig. 6 models) and decreases by factors of 5. As in figure 6, <i>t</i> =0 corresponds to	Formatted: Font: Italic
1 1976	an equilibrium condition where the initial slope and initial threshold are consistent with the	
1977	initial upstream sediment supply. Slope and $\tau_{c(q_i)}^*$ were averaged over nodes 3-10, leaving out	Deleted:
1978	the first and last two nodes because of minor model boundary effects.	Deleted: $ au_c^*$
I 1979		Deleted:
1		
1980	Figure 8 Morphodynamic model sensitivity to sediment supply perturbations and k. All	Deleted:
1981	models started at the same equilibrium condition as shown in Fig. 6 and 7 a. Slope	Deleted:
1982	adjustment, normalized by the initial equilibrium slope. The correspondence of Eq. 20 and the	Deleted: 17
1983	morphodynamic model calculations demonstrate that the models did asymptotically attain	Deleted
1984	equilibrium slopes. b. $S_{eq}$ ratio is the ratio of equilibrium slopes of the Exner+ $ au_{c(q_s)}^*$ model	Deleted:
		Deleted: $ au_c^*$
1985	divided by $S_{eq}$ for the Exner-only model, to show the relative affect that that $\tau_c^*$ evolution has	Deleted:
1986	on equilibrium slopes. c. Equilibrium timescales for model adjustment d. teq ratio is the ratio	Deleted: $ au_c^*$
1987	of $t_{eq}$ for the Exner+ $\tau_{c(q_s)}^*$ model divided by $t_{eq}$ for the Exner-only model. Values are lower	Deleted:
1988	than 1, indicating that the $\tau_c^*$ evolution has a large influence on equilibrium timescales. e.	Deleted: $ au_c^*$
1900		Deleted:
1989	Evolution of $\tau_{c(q_s)}^*$ .	Deleted:
1000		Deleted:
1990		Formatted: Font: Italic
1991	Figure 9 Spatial and temporal evolution of morphodynamic slopes, for the same models	Deleted:
1992	shown in Fig. 6. Slope is initially at equilibrium and responds to the 5x increase in upstream	Deleted:
1993	sediment supply at $t=0$ a. The Exner-only model initially has spatial slope variability, but	Deleted:
1994	evolves to a uniform new equilibrium slope. b, c. In the Exner+ $\tau_{c(q_i)}^*$ model, spatial variability	<b>Deleted:</b> with evolving $ au_c^*$
1995	<u>in both</u> slope and $\tau_{c(q_s)}^*$ persist even at equilibrium.	<b>Deleted:</b> $ au_c^*$ variability
	- (vg <sub>S</sub> )	Deleted:



Deleted:

Formatted: Font: Italic

Formatted: Font: Italic, Subscript

**Deleted:** Figure 11. Comparison of Reynolds creek and  $au_c^*$  data compilation predictions using Eq. (18) and (21). a. Longitudinal profile based on airborne Lidar (Olinde, 2015). Upstream end (distance=0) is an arbitrary location along the channel (a bridge). Data gap at 730 m is a gauging station weir; the slope steepens downstream of the weir where the valley becomes constricted by bedrock, although the bed remains almost entirely alluvial. b. Slopes calculated (averaged) over 100 m reaches, illustrating reach-scale slope variability. c. Histogram of  $au_c^*$  compilation (data shown in Fig. 1), compared to  $au_c^*$  calculated using Eq. (21), based on Reynolds Creek 100 m slopes (panel b), and assuming  $q_w$ =1 m2/s,  $q_s^*$ =2e-3, and f=0.1. d. Similar calculation as panel c, but using Eq. 18 to solve for slope as a function of  $au_c^*$  from the Fig. 1 data compilation, and compared to panel b slopes.¶

### References

2051

- 2052 Ancey, C., Davison, A. C., Bohm, T., Jodeau, M., and Frey, P.: Entrainment and motion of
- 2053 coarse particles in a shallow water stream down a steep slope, Journal of Fluid Mechanics,
- 2054 595, 83-114, doi:10.1017/s0022112007008774, 2008.
- 2055 Buffington, J. M., and Montgomery, D. R.: A systematic analysis of eight decades of incipient
- 2056 motion studies, with special reference to gravel-bedded rivers, Water Resources Research, 33,
- 2057 1993-2029, doi:10.1029/97wr03190, 1997.
- 2058 Buffington, J. M.: The legend of A. F. Shields, Journal of Hydraulic Engineering-Asce, 125,
- 2059 376-387, doi:10.1061/(asce)0733-9429(1999)125:4(376), 1999.
- 2060 Bunte, K., Abt, S. R., Swingle, K. W., Cenderelli, D. A., and Schneider, J. M.: Critical
- 2061 Shields values in coarse-bedded steep streams, Water Resources Research, 49, 7427-7447,
- 2062 doi:10.1002/2012wr012672, 2013.
- 2063 Buscombe, D., and Conley, D. C.: Effective shear stress of graded sediments, Water
- 2064 Resources Research, 48, 13, doi:10.1029/2010wr010341, 2012.
- 2065 Celik, A. O., Diplas, P., Dancey, C. L., and Valyrakis, M.: Impulse and particle dislodgement
- under turbulent flow conditions, Physics of Fluids, 22, doi:10.1063/1.3385433, 2010.
- 2067 Chen, L., and Stone, M. C.: Influence of bed material size heterogeneity on bedload transport
- 2068 uncertainty, Water Resources Research, 44, doi:10.1029/2006wr005483, 2008.
- 2069 Chin, A., and Phillips, J. D.: The self-organization of step-pools in mountain streams,
- 2070 Geomorphology, 83, 346-358, doi:10.1016/j.geomorph.2006.02.021, 2007.
- 2071 Chiu, C. L.: Entropy and Probability Concepts in Hydraulics, Journal of Hydraulic
- 2072 Engineering, 113, 583-599, doi:doi:10.1061/(ASCE)0733-9429(1987)113:5(583), 1987.
- 2073 Church, M., Hassan, M. A., and Wolcott, J. F.: Stabilizing self-organized structures in gravel-
- 2074 bed stream channels: Field and experimental observations, Water Resources Research, 34,
- 2075 3169-3179, doi:10.1029/98wr00484, 1998.
- 2076 Church, M.: Bed material transport and the morphology of alluvial river channels, Annual
- 2077 Review of Earth and Planetary Sciences, 34, 325-354,
- 2078 doi:10.1146/annurev.earth.33.092203.122721, 2006.
- 2079 Curran, J. C., and Wilcock, P. R.: Effect of sand supply on transport rates in a gravel-bed
- 2080 channel, Journal of Hydraulic Engineering-Asce, 131, 961-967, doi:10.1061/(asce)0733-
- 2081 9429(2005)131:11(961), 2005.
- 2082 David, G. C. L., Wohl, E., Yochum, S. E., and Bledsoe, B. P.: Comparative analysis of bed
- 2083 resistance partitioning in high-gradient streams, Water Resources Research, 47,
- 2084 doi:10.1029/2010wr009540, 2011.
- 2085 Dietrich, W. E., Kirchner, J. W., Ikeda, H., and Iseya, F.: Sediment supply and the
- development of the coarse surface-layer in gravel-bedded rivers, Nature, 340, 215-217,
- 2087 doi:10.1038/340215a0, 1989.
- 2088 Diplas, P., Dancey, C. L., Celik, A. O., Valyrakis, M., Greer, K., and Akar, T.: The Role of
- 2089 Impulse on the Initiation of Particle Movement Under Turbulent Flow Conditions, Science,
- 2090 322, 717-720, doi:10.1126/science.1158954, 2008.

- 2091 Fonstad, M. A.: Spatial variation in the power of mountain streams in the Sangre de Cristo
- 2092 Mountains, New Mexico, Geomorphology, 55, 75-96, doi:10.1016/s0169-555x(03)00133-8,
- 2093 2003.
- 2094 Furbish, D. J., Haff, P. K., Roseberry, J. C., and Schmeeckle, M. W.: A probabilistic
- description of the bed load sediment flux: 1. Theory, J. Geophys. Res.-Earth Surf., 117, 21,
- 2096 doi:10.1029/2012jf002352, 2012.
- 2097 Gilbert, G. K.: The transportation of debris by running water, United States Geological
- 2098 Survey Professional Paper, 86, 1914.
- 2099 Gogus, M., and Defne, Z.: Effect of shape on incipient motion of large solitary particles,
- 2100 Journal of Hydraulic Engineering-Asce, 131, 38-45, doi:10.1061/(asace)0733-
- 2101 9429(2005)131:1(38), 2005.
- 2102 Gomez, B., and Church, M.: As assessment of bed load sediment transport formulae for
- 2103 gravel rivers, Water Resources Research, 25, 1161-1186, doi:10.1029/WR025i006p01161,
- 2104 1989
- 2105 Hemond, H. F., and Fechner, E. J.: Chemical fate and transport in the environment, Elsevier,
- 2106 2014.
- 2107 Iseya, F., and Ikeda, H.: Pulsations in Bedload Transport Rates Induced by a Longitudinal
- 2108 Sediment Sorting a Flume Study Using Sand and Gravel Mixtures, Geogr. Ann. Ser. A-
- 2109 Phys. Geogr., 69, 15-27, 1987.
- 2110 Jackson, W. L., and Beschta, R. L.: Influences of increased sand delivery on the morphology
- 2111 of sand and gravel channels, JAWRA Journal of the American Water Resources Association,
- 2112 20, 527-533, doi:10.1111/j.1752-1688.1984.tb02835.x, 1984.
- 2113 Jerolmack, D. J.: Causes and effects of noise in landscape dynamics, Eos, Transactions
- 2114 American Geophysical Union, 92, 385-386, doi:10.1029/2011EO440001, 2011.
- 2115 Johnson, J. P. L., Aronovitz, A. C., and Kim, W.: Coarser and rougher: Effects of fine gravel
- pulses on experimental step-pool channel morphodynamics, Geophys. Res. Lett., 42, 8432-
- 2117 8440, doi:10.1002/2015gl066097, 2015.
- 2118 Kirchner, J. W., Dietrich, W. E., Iseya, F., and Ikeda, H.: The Variability of Critical Shear-
- 2119 Stress, Friction Angle, and Grain Protrusion in Water-Worked Sediments, Sedimentology, 37,
- 2120 647-672, doi:10.1111/j.1365-3091.1990.tb00627.x, 1990.
- 2121 Kleidon, A.: A basic introduction to the thermodynamics of the Earth system far from
- equilibrium and maximum entropy production, Philos. Trans. R. Soc. B-Biol. Sci., 365, 1303-
- 2123 1315, doi:10.1098/rstb.2009.0310, 2010.
- 2124 Lamb, M. P., Dietrich, W. E., and Venditti, J. G.: Is the critical Shields stress for incipient
- sediment motion dependent on channel-bed slope?, Journal of Geophysical Research, 113,
- 2126 F02008, doi:10.1029/2007jf000831, 2008.
- 2127 Lenzi, M. A., Mao, L., and Comiti, F.: When does bedload transport begin in steep boulder-
- 2128 bed streams?, Hydrological Processes, 20, 3517-3533, doi:10.1002/hyp.6168, 2006.
- 2129 Leopold, L. B., and Langbein, W. B.: The concept of entropy in landscape evolution, US
- 2130 Government Printing Office Washington, DC, USA, 1962.
- 2131 Mackin, J. H.: Concept of the graded river, Geol. Soc. Am. Bull., 101, 1373-1388, 1948.

- 2132 Mao, L. C.: The effect of hydrographs on bed load transport and bed sediment spatial
- 2133 arrangement, J. Geophys. Res.-Earth Surf., 117, doi:10.1029/2012jf002428, 2012.
- 2134 Marquis, G. A., and Roy, A. G.: Using multiple bed load measurements: Toward the
- 2135 identification of bed dilation and contraction in gravel-bed rivers, J. Geophys. Res.-Earth
- 2136 Surf., 117, 16, doi:10.1029/2011jf002120, 2012.
- 2137 Martin, R. L., Jerolmack, D. J., and Schumer, R.: The physical basis for anomalous diffusion
- 2138 in bed load transport, J. Geophys. Res.-Earth Surf., 117, 18, doi:10.1029/2011jf002075, 2012.
- 2139 Martin, R. L., and Jerolmack, D. J.: Origin of hysteresis in bed form response to unsteady
- 2140 flows, Water Resources Research, 49, 1314-1333, doi:10.1002/wrcr.20093, 2013.
- Measures, R., and Tait, S.: Quantifying the role of bed surface topography in controlling
- 2142 sediment stability in water-worked gravel deposits, Water Resources Research, 44,
- 2143 doi:10.1029/2006wr005794, 2008.
- 2144 Meyer-Peter, E., and Müller, R.: Formulas for bed-load transport, Proceedings, Second
- 2145 Congress, International Association for Hydraulic Structures Research, Stockholm, 39-64,
- 2146 1948.
- Nelson, P. A., Venditti, J. G., Dietrich, W. E., Kirchner, J. W., Ikeda, H., Iseya, F., and Sklar,
- 2148 L. S.: Response of bed surface patchiness to reductions in sediment supply, J. Geophys. Res.-
- 2149 Earth Surf., 114, doi:10.1029/2008jf001144, 2009.
- 2150 Nitsche, M., Rickenmann, D., Turowski, J. M., Badoux, A., and Kirchner, J. W.: Evaluation
- 2151 of bedload transport predictions using flow resistance equations to account for macro-
- 2152 roughness in steep mountain streams, Water Resources Research, 47,
- 2153 doi:10.1029/2011wr010645, 2011.
- 2154 Ockelford, A.-M., and Haynes, H.: The impact of stress history on bed structure, Earth
- 2155 Surface Processes and Landforms, 38, 717-727, doi:10.1002/esp.3348, 2013.
- 2156 Olinde, L.: Displacement and entrainment behavior of bedload clasts in mountain streams,
- 2157 Ph.D., Geological Sciences, The University of Texas at Austin, Austin, Texas, 139 pp., 2015.
- 2158 Olinde, L., and Johnson, J. P. L.: Using RFID and accelerometer-embedded tracers to
- 2159 measure probabilities of bed load transport, step lengths, and rest times in a mountain stream,
- 2160 Water Resources Research, 51, 7572-7589, doi:10.1002/2014wr016120, 2015.
- 2161 Oxtoby, D., Gillis, H., and Butler, L.: Principles of modern chemistry, Cengage Learning,
- 2162 2015.
- 2163 Paik, K., and Kumar, P.: Optimality approaches to describe characteristic fluvial patterns on
- 2164 landscapes, Philos. Trans. R. Soc. B-Biol. Sci., 365, 1387-1395, doi:10.1098/rstb.2009.0303,
- 2165 2010.
- 2166 Paola, C., and Voller, V. R.: A generalized Exner equation for sediment mass balance, J.
- 2167 Geophys. Res.-Earth Surf., 110, F04014, doi:10.1029/2004JF000274., 2005.
- 2168 Parker, G., and Klingeman, P. C.: On Why Gravel Bed Streams Are Paved, Water Resources
- 2169 Research, 18, 1409-1423, doi:10.1029/WR018i005p01409, 1982.
- 2170 Parker, G., Klingeman, P. C., and McLean, D. G.: Bedload size distribution in paved gravel-
- bed streams, American Society of Civil Engineers, Journal of Hydraulics Division, 108, 1757-
- 2172 1760, 1982.

- 2173 Parker, G.: Surface-based bedload transport relation for gravel rivers, Journal of Hydraulic
- 2174 Research, 28, 417-436, doi:10.1080/00221689009499058, 1990.
- 2175 Parker, G., and Toro-Escobar, C. M.: Equal mobility of gravel in streams: The remains of the
- 2176 day, Water Resources Research, 38, doi:10.1029/2001wr000669, 2002.
- 2177 Phillips, C. B., Martin, R. L., and Jerolmack, D. J.: Impulse framework for unsteady flows
- 2178 reveals superdiffusive bed load transport, Geophys. Res. Lett., 40, 1328-1333,
- 2179 doi:10.1002/grl.50323, 2013.
- 2180 Phillips, J. D.: Multiple modes of adjustment in unstable river channel cross-sections, Journal
- 2181 of Hydrology, 123, 39-49, doi:10.1016/0022-1694(91)90067-R, 1991.
- 2182 Phillips, J. D.: The perfect landscape, Geomorphology, 84, 159-169
- 2183 doi:10.1016/j.geomorph.2006.01.039, 2007.
- 2184 Phillips, J. D.: Changes, perturbations, and responses in geomorphic systems, Progress in
- 2185 Physical Geography, 33, 17-30, doi:10.1177/0309133309103889, 2009.
- 2186 Phillips, J. D.: Emergence and pseudo-equilibrium in geomorphology, Geomorphology, 132,
- 2187 319-326, doi:10.1016/j.geomorph.2011.05.017, 2011.
- Powell, D. M., and Ashworth, P. J.: Spatial pattern of flow competence and bed-load transport
- 2189 in a divided gravel-bed river, Water Resources Research, 31, 741-752
- 2190 doi:10.1029/94wr02273, 1995.
- 2191 Prancevic, J. P., and Lamb, M. P.: Unraveling bed slope from relative roughness in initial
- 2192 sediment motion, J. Geophys. Res.-Earth Surf., 120, 474-489, doi:10.1002/2014jf003323,
- 2193 2015.
- 2194 Recking, A.: Influence of sediment supply on mountain streams bedload transport,
- 2195 Geomorphology, 175, 139-150, doi:10.1016/j.geomorph.2012.07.005, 2012.
- 2196 Richards, K., and Clifford, N.: Fluvial geomorphology: structured beds in gravelly rivers,
- 2197 Progress in Physical Geography, 15, 407-422, doi:10.1177/030913339101500404, 1991.
- 2198 Rickenmann, D.: Comparison of bed load transport in torrents and gravel bed streams, Water
- 2199 Resources Research, 37, 3295-3305, doi:10.1029/2001WR000319, 2001.
- 2200 Rickenmann, D., and Recking, A.: Evaluation of flow resistance in gravel-bed rivers through
- a large field data set, Water Resources Research, 47, doi:10.1029/2010wr009793, 2011.
- 2202 Rodriguez-Iturbe, I., and Rinaldo, A.: Fractal River Networks: Chance and Self-
- 2203 Organization, Cambridge University Press, New York, 1997.
- 2204 Sanguinito, S., and Johnson, J.: Quantifying gravel overlap and dislodgement forces on
- 2205 natural river bars: implications for particle entrainment, Earth Surface Processes and
- 2206 Landforms, 37, 134-141, doi:10.1002/esp.2237, 2012.
- 2207 Schmeeckle, M. W., and Nelson, J. M.: Direct numerical simulation of bedload transport
- using a local, dynamic boundary condition, Sedimentology, 50, 279-301, doi:10.1046/j.1365-
- 2209 3091.2003.00555.x, 2003.
- 2210 Schneider, J. M., Rickenmann, D., Turowski, J. M., Bunte, K., and Kirchner, J. W.:
- 2211 Applicability of bed load transport models for mixed-size sediments in steep streams
- 2212 considering macro-roughness, Water Resources Research, 51, 5260-5283,
- 2213 doi:10.1002/2014wr016417, 2015.

- 2214 Shvidchenko, A. B., and Pender, G.: Flume study of the effect of relative depth on the
- 2215 incipient motion of coarse uniform sediments, Water Resources Research, 36, 619-628,
- 2216 doi:10.1029/1999wr900312, 2000.
- 2217 Sklar, L. S., Fadde, J., Venditti, J. G., Nelson, P., Wydzga, M. A., Cui, Y. T., and Dietrich, W.
- 2218 E.: Translation and dispersion of sediment pulses in flume experiments simulating gravel
- augmentation below dams, Water Resources Research, 45, doi:10.1029/2008wr007346, 2009.
- 2220 Stark, C. P., and Stark, G. J.: A channelization model of landscape evolution, American
- 2221 Journal of Science, 301, 486-512, doi:10.2475/ajs.301.4-5.486, 2001.
- 2222 Strom, K. B., and Papanicolaou, A. N.: Occurrence of cluster microforms in mountain rivers,
- 2223 Earth Surface Processes and Landforms, 34, 88-98, doi:10.1002/esp.1693, 2009.
- 2224 Turowski, J. M., Badoux, A., and Rickenmann, D.: Start and end of bedload transport in
- 2225 gravel-bed streams, Geophys. Res. Lett., 38, L04401, doi:10.1029/2010gl046558, 2011.
- 2226 Valyrakis, M., Diplas, P., Dancey, C. L., Greer, K., and Celik, A. O.: Role of instantaneous
- 2227 force magnitude and duration on particle entrainment, J. Geophys. Res.-Earth Surf., 115,
- 2228 doi:10.1029/2008jf001247, 2010.
- 2229 Venditti, J. G., Dietrich, W. E., Nelson, P. A., Wydzga, M. A., Fadde, J., and Sklar, L.:
- 2230 Mobilization of coarse surface layers in gravel-bedded rivers by finer gravel bed load, Water
- 2231 Resour. Res., 46, doi:10.1029/2009wr008329, 2010.
- 2232 Wilcock, P. R., and Crowe, J. C.: Surface-based transport model for mixed-size sediment,
- 2233 Journal of Hydraulic Engineering-Asce, 129, 120-128, doi:10.1061/(asce)0733-
- 2234 9429(2003)129:2(120), 2003.
- 2235 Wong, M., and Parker, G.: Reanalysis and Correction of Bed-Load Relation of Meyer-Peter
- and Müller Using Their Own Database, Journal of Hydraulic Engineering, 132, 1159-1168,
- 2237 doi:doi:10.1061/(ASCE)0733-9429(2006)132:11(1159), 2006.
- 2238 Yager, E. M., Dietrich, W. E., Kirchner, J. W., and McArdell, B. W.: Prediction of sediment
- transport in step-pool channels, Water Resources Research, 48, doi:10.1029/2011wr010829,
- 2240 2012a.

2246

- 2241 Yager, E. M., Turowski, J. M., Rickenmann, D., and McArdell, B. W.: Sediment supply,
- 2242 grain protrusion, and bedload transport in mountain streams, Geophys. Res. Lett., 39,
- 2243 doi:10.1029/2012gl051654, 2012b.
- 2244 Yanites, B. J., and Tucker, G. E.: Controls and limits on bedrock channel geometry, J.
- 2245 Geophys. Res.-Earth Surf., 115, 17, doi:10.1029/2009jf001601, 2010.